



Norwegian University of
Science and Technology

Direct Numerical Simulation of Turbulent Channel Flow

Benjamin Clement Sebastian

Master of Energy and Environmental Engineering

Submission date: June 2018

Supervisor: Helge Ingolf Andersson, EPT

Co-supervisor: Lihao Zhao, EPT

Norwegian University of Science and Technology
Department of Energy and Process Engineering

EPT-M-2018-78

MASTER THESIS

for

Student Benjamin Clement Sebastian

Spring 2018

Direct numerical simulation of turbulent channel flow

*Direkte numerisk simulering av turbulent kanalstrømning***Background and objective**

The Navier-Stokes equations are known to give a complete representation also of turbulent flows. In direct numerical simulations (DNSs), this mathematical model is solved in time and three-dimensional space on a computational grid with mesh size smaller than the tiniest turbulent eddies. An exact representation of a turbulent flow field on discrete grid points can only be obtained by means of DNS. The objective of the project is to familiarize the candidate with an in-house DNS code and how to operate it on a parallel computer. A crucial part of DNS-based research is the definition of the computational problem, i.e. relevant boundary conditions, choice of computational domain, and design of computational mesh.

The following tasks are to be considered:

- 1 In-depth study of the pioneering article by Kim, Moin & Moser in J. Fluid Mech. (1987).
- 2 Perform coarse-grid trial simulations and compare with existing data.
- 3 Perform short-domain trial simulations and compare with existing data.
- 4 Perform narrow-domain trial simulations and compare with existing data.
- 5 Analyze and discuss the influence of domain size (length, width) and grid resolution.
- 6 Give guidelines for the required domain size and grid resolution.
- 7 Discuss Reynolds number effects (if the time allows).

Within 14 days of receiving the written text on the master thesis, the candidate shall submit a research plan for his project to the department.

When the thesis is evaluated, emphasis is put on processing of the results, and that they are presented in tabular and/or graphic form in a clear manner, and that they are analyzed carefully.

The thesis should be formulated as a research report with summary both in English and Norwegian, conclusion, literature references, table of contents etc. During the preparation of the text, the candidate should make an effort to produce a well-structured and easily readable report. In order to ease the evaluation of the thesis, it is important that the cross-references are correct. In the making of the report, strong emphasis should be placed on both a thorough discussion of the results and an orderly presentation.

The candidate is requested to initiate and keep close contact with his/her academic supervisor(s) throughout the working period. The candidate must follow the rules and regulations of NTNU as well as passive directions given by the Department of Energy and Process Engineering.

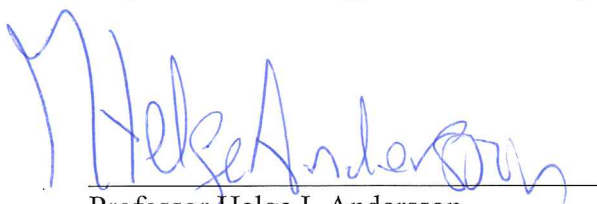
Risk assessment of the candidate's work shall be carried out according to the department's procedures. The risk assessment must be documented and included as part of the final report. Events related to the candidate's work adversely affecting the health, safety or security, must be documented and included as part of the final report. If the documentation on risk assessment represents a large number of pages, the full version is to be submitted electronically to the supervisor and an excerpt is included in the report.

Pursuant to “Regulations concerning the supplementary provisions to the technology study program/Master of Science” at NTNU §20, the Department reserves the permission to utilize all the results and data for teaching and research purposes as well as in future publications.

The final report is to be submitted digitally in DAIM. An executive summary of the thesis including title, student's name, supervisor's name, year, department name, and NTNU's logo and name, shall be submitted to the department as a separate pdf file. Based on an agreement with the supervisor, the final report and other material and documents may be given to the supervisor in digital format.

- Work to be done in lab (Water power lab, Fluids engineering lab, Thermal engineering lab)
- Field work

Department of Energy and Process Engineering, 15. January 2018



Professor Helge I. Andersson
Academic Supervisor

Research Advisor:

Dr Lihao Zhao, Associate Professor, Tsinghua University (Beijing) and NTNU (Trondheim)

ABSTRACT

Several Direct Numerical Simulations (DNS) of a fully developed turbulent channel flow are performed. The aim of this thesis is to analyze how grid resolutions and domain sizes affect the turbulence statistics. The simulations have been divided into four cases with a variable number of simulations within each case: Coarse-grid, Short-domain, Narrow-domain and Large-domain. The simulations, in each case, are compared to both each other and to the results obtained by Kim et al.[1]. The latter is used as a reference and is considered very accurate. The friction Reynolds number of the flow, which is based on the channel height, is 360.

The **Coarse-grid** case consists of three simulations with grid resolutions of $24 \times 24 \times 96$, $48 \times 24 \times 96$ and $48 \times 48 \times 192$, in x , y and z respectively. The domain size is kept constant at $l_x = 1.5$, $l_y = 0.75$ and $l_z = 1$, where l_x , l_y and l_z is the channel length, width and height, respectively. The results obtained in this case indicates that the grid resolution of $24 \times 24 \times 96$ is too coarse and that the domain size is too small. The results are therefore unreliable. For the **Short-domain** case the channel length is doubled twice to $l_x = 3$ and $l_x = 6$ and the grid resolution in the streamwise direction is increased accordingly to keep the resolution constant. Domain size effect is the expected outcome for this case. The results show expected data for the large scale motion compared to Kim et al.[1]. The small scale motion show a grid effect between the simulations of length $l_x = 1.5$ and $l_x = 3$. Between the channels of length $l_x = 3$ and $l_x = 6$ the discrepancy is less. The two longest channels show satisfying results, even though the two-point correlation deviates from zero. In the **Narrow-domain** case the channel width is doubled two times, while keeping the length constant. The results are satisfying for the large scale motion. The small scale motion shows smaller discrepancies compared to each other and bigger discrepancies compared to Kim et al.[1] than for the Short-domain case. This suggests that there is a small or non-existent grid effect. The two-point correlation shows that only the widest channel is adequate. The **Large-domain** case consists of a simulation with grid resolution of $192 \times 192 \times 192$ and domain size $l_x = 6$ and $l_y = 3$. The turbulence statistics correspond well with Kim et al.[1] and the two-point correlation shows that the domain size is adequate in both directions. The discrepancies are small compared to the Short-domain case, which indicates that the simulations in Short-domain case yields satisfying results. This suggests that increasing the channel length will yield better results and have greater impact than increasing the channel width.

SAMMENDRAG

Formålet med oppgaven er å gjennomføre en serie med Direkte Numeriske Simuleringer (DNS) av en fullt utviklet turbulent kanalstrømning for å analysere hvordan ulike gridoppløsninger og domenestørrelser påvirker turbulensen. Simuleringene har blitt delt opp i ulike tilfeller, med flere simuleringer per tilfelle: Grovt-grid, Kort-domene, Smalt-domene og Stort-domene. Simuleringene i hvert tilfelle sammenliknes både med hverandre og med arbeidet gjort av Kim et al.[1]. Sistnevnte er brukt som referanse og er ansett for å være nøyaktig. Strømningen har et friksjons-Reynoldstall på 360, som er basert på kanalhøyden. **Grovt-grid** består av tre simuleringer med gridoppløsning på $24 \times 24 \times 96$, $48 \times 24 \times 96$ og $48 \times 48 \times 192$ i x, y og z. Domenestørrelsen er konstant lik $l_x = 1.5$, $l_y = 0.75$ og $l_z = 1$ gjennom simuleringene. Formålet er å se effekten av økende gridoppløsning. Resultatene indikerer at den grovste gridoppløsningen er for grov og domenestørrelsen for liten, og fører til upålitelige data. **Kort-domenetilfellet** består av to simuleringer hvor kanallengden er doblet to ganger. Oppløsningen er den samme, det vil si at gridoppløsningen i strømretningen også dobles to ganger. Det gjør at det i utgangspunktet kun skal være en domeneeffekt. Dette gjelder også for Smalt-domenetilfellet. Resultatene viser en liten, men gradvis forbedring for storskalaturbulensen. For småskalaturbulensen er det merkbare forskjeller spesielt mellom simuleringene med lengde $l_x = 1.5$ og $l_x = 3$, men mindre forskjeller mellom $l_x = 3$ og $l_x = 6$. Det tyder på at en grideffekt har oppstått mellom de to førstnevnte simuleringene og en mindre grideffekt for de to sistnevnte. Ellers ser resultatene ut til å korrespondere bra med Kim et al.[1]. Resultatene virker å være tilfredsstillende, selv om to-punktskorrelasjonen viser et avvik for begge simuleringene. Det neste tilfellet, **Smalt-domene**, dobler bredden på kanalen to ganger. Resultatet for storskalaturbulensen viser liten endring mellom simuleringene, men har merkbare forskjeller fra Kim et al.[1]. For småskalaturbulensen er det heller ikke stor endring mellom simuleringene og tyder på at det er liten eller ikke-eksisterende grideffekt. Resultatene er dårligere enn for Kort-domenetilfellet. To-punktskorrelasjonen viser at kanalbredden er tilstrekkelig for det bredeste tilfellet. **Stort-domene** består av en simulering med domenestørrelse $l_x = 6$ og $l_y = 3$ og gridoppløsning på $192 \times 192 \times 192$. Domenestørrelsen er veldig nært det som er brukt i Kim et al.[1]. Både storskala- og småskala turbulens viser resultater tilsvarende det lengste domenet i Kort-domenetilfellet. To-punktskorrelasjonen indikerer at domenestørrelsen er tilstrekkelig. Dette gir en indikasjon på at økning i bredden har mindre betydning enn økning i lengden. Det betyr at simuleringene i Kort-domene gir tilfredsstillende resultater.

PREFACE

This thesis ends a five year Master program in Energy and Environmental Engineering at NTNU.

The work done in this thesis is a continuation of the project work during the fall of 2017. Most of the theory was therefore taken from the project work, after consultation with my academic supervisor. The work performed in this thesis has been very exciting and challenging at the same time. It was exciting to learn in-depth how DNS works in practice.

I would like to thank my academic supervisor Professor Helge I. Andersson and my research advisor Dr. Lihao Zhao for valuable guidance and discussions. Thank you for all the help you have provided me.

I would also want to thank my family for their endless love, support and encouragement throughout my years at NTNU. You have always believed in me and for that I am grateful. Last, I want to thank all my friends for their support and encouragement.

Trondheim, June 2018.
Benjamin Clement Sebastian

CONTENTS

ABSTRACT	iii
SAMMENDRAG	v
PREFACE	vii
NOTATION	xv
1 INTRODUCTION	1
1.1 Background in turbulent flows	1
I RESEARCH METHODOLOGY	3
2 THEORY	5
2.1 Equations of motion	5
2.2 Turbulent equations of motion	6
2.2.1 Reynolds decomposition	7
2.2.2 Equations for the mean flow	8
2.2.3 Equations for the turbulent fluctuations	10
2.2.4 Viscosity and dissipation	11
2.3 Reynolds stress	11
2.4 Turbulent scales and energy conversion	12
2.5 Pioneering article by Kim et al.(1987)	14
3 FLOW DOMAIN AND GEOMETRY	17
3.1 Channel flow	17
3.2 Flow along a solid surface	18
4 NUMERICAL SOLUTIONS	23
4.1 Direct Numerical Simulation	23
4.2 Equations solved	23
4.3 Pressure-velocity coupling	24
4.4 Discretization Schemes	24
4.4.1 Spatial derivatives in homogeneous directions	25
4.4.2 Spatial derivatives in wall-normal direction	26
4.4.3 Temporal discretization	27
4.4.4 Boundary and Initial conditions	28
4.5 Computational mesh and domain	29
4.5.1 Coarse-grid simulations	29
4.5.2 Short-domain simulations	29
4.5.3 Narrow-domain simulations	30

4.5.4	Large-domain simulations	30
II	RESULTS	33
5	RESULTS	35
5.1	Coarse grid simulations	35
5.1.1	Mean properties	35
5.1.2	Turbulence intensities	38
5.1.3	Reynolds shear stress	40
5.1.4	Vorticity	41
5.1.5	Dissipation	43
5.2	Short domain simulations	46
5.2.1	Mean properties	47
5.2.2	Turbulence intensities	48
5.2.3	Reynolds shear stress	50
5.2.4	Vorticity	51
5.2.5	Dissipation	52
5.2.6	Two-point correlation	53
5.3	Narrow domain simulations	55
5.3.1	Turbulence intensities	56
5.3.2	Reynolds shear stress	57
5.3.3	Vorticity	58
5.3.4	Dissipation	59
5.3.5	Two-point correlation	60
5.4	Large-domain simulations	62
5.4.1	Two-point correlation	65
III	DISCUSSION AND CONCLUSION	67
6	DISCUSSION	69
6.1	Discussion	69
6.1.1	Coarse-grid simulations	69
6.1.2	Short-domain simulations	70
6.1.3	Narrow-domain simulations	71
6.1.4	Large-domain simulations	71
6.1.5	Guidelines for required domain size and grid resolution	72
6.1.6	Further work	72
7	CONCLUSION	73
	Bibliography	75

LIST OF FIGURES

Figure 1	Geometry and coordinate system of the flow	18
Figure 2	u_{192}^+ plotted against different wall region layers in $\log z^+$.	20
Figure 3	Discretized grid in wall normal direction. The black filled circles represent the cell centers, while the unfilled circles represent the cell faces.	25
Figure 4	Normalized mean velocity profile for different simulations compared with data from Kim et al.[1]	36
Figure 5	Velocity profile close to the wall, in logarithmic scale, compared with data from [1]	37
Figure 6	The rms values of the velocity fluctuations for different simulations compared with data from [1]	39
Figure 7	The viscous, turbulent and total shear stress for increasing grid resolutions compared with data from [1]	41
Figure 8	The rms value of the vorticity fluctuations for increasing grid resolutions compared with data from [1]	43
Figure 9	The dissipation components for increasing grid resolutions compared with data from [1]	45
Figure 10	The total dissipation for increasing grid resolutions compared with data from [1]	46
Figure 11	The mean velocity profile for the Short-domain case for increasing streamwise domain size, l_x , compared with data from Kim et al.[1]	48
Figure 12	The rms value of the velocity fluctuations for the Short-domain case for increasing streamwise domain size, l_x , compared with data from Kim et al.[1]	49
Figure 13	The Reynolds shear stress, viscous shear stress and total shear stress for the Short-domain case for increasing streamwise domain size compared with data from Kim et al.[1]	50
Figure 14	The rms value of the vorticity fluctuations for the Short-domain case for increasing streamwise domain size compared with data from [1]	51
Figure 15	The dissipation components and total dissipation for the Short-domain case for increasing streamwise domain size compared with data from Kim et al.	52

Figure 16	Two-point correlation in the streamwise direction for increased values of l_x at the center of the channel.	54
Figure 17	Two-point correlation in the spanwise direction for increased values of l_x at the center of the channel.	55
Figure 18	Turbulence intensities for increasing channel width l_y .	57
Figure 19	Viscous, turbulent and total shear stress for increasing values of domain width l_y .	58
Figure 20	Rms of vorticity for increasing values of domain width l_y .	59
Figure 21	The dissipation components and the total dissipation for the Narrow-domain case for increasing values of the width compared with data from Kim et al.	60
Figure 22	Two-point correlation in the streamwise direction for increased values of l_x at the center of the channel.	61
Figure 23	Two-point correlation in the spanwise direction for increased values of l_x at the center of the channel.	62
Figure 24	Mean velocity profile, rms values of the velocity fluctuations, turbulent-, viscous- and total shear stress, and rms values of the vorticity for the domain size $l_x = 6$ and $l_y = 3$.	64
Figure 25	The dissipation components and the total dissipation for the Large-domain case compared with data from Kim et al.	65
Figure 26	Two-point correlation for both the streamwise and spanwise directions for domain sizes of $l_x = 6$ and $l_y = 3$.	66

LIST OF TABLES

Table 1	Wall region layers ([2], p. 275)	21
Table 2	Grid resolutions and domain size for the Coarse-domain case	30
Table 3	Grid resolutions and domain size for the Short-domain case	30
Table 4	Grid resolutions and domain size for the Narrow-domain case	30
Table 5	Grid resolutions and domain size for the Large-domain case	31

NOTATION

ρ	Density
u_i	Velocity in i direction
u	Velocity in x direction
v	Velocity in y direction
w	Velocity in z direction
ω_i	Vorticity in i direction
σ_{ij}	Stress tensor
p	Pressure
δ_{ij}	Kronecker delta
μ	Viscosity
μ_B	Bulk viscosity
ν	Kinematic viscosity
λ	Second viscosity coefficient
\tilde{a}	Represents instantaneous values
A	Capital variables means averaged values
a	Small variables means fluctuating values
s_{ij}	Rate of strain tensor
σ_{ij}	Stress tensor
τ_{ij}	Reynolds stress tensor
k	Kinetic energy
ϵ	Total dissipation rate of turbulent kinetic energy
ϵ_{ij}	Dissipation tensor
η	Kolmogorov length scale
u_η	Kolmogorov's micro scale, velocity
τ_η	Kolmogorov's micro scale, time
ℓ_0	Integral scale, length
u_{ℓ_0}	Integral scale, velocity
τ_0	Integral scale, time
u_τ	Friction velocity
Re_τ	Friction Reynolds number
x	Streamwise coordinate
y	Spanwise coordinate
z	Wall-normal coordinate
z^+	Wall distance

l_x	Channel length
l_y	Channel width
l_z	Channel height
u^+	Mean velocity normalized by friction velocity
$u_{i,rms}$	Rms value for i-component of velocity fluctuation
$\omega_{i,rms}$	Rms value for i-component of vorticity fluctuation

INTRODUCTION

1.1 BACKGROUND IN TURBULENT FLOWS

As is clear from the problem formulation given earlier, this thesis will address different aspects of Direct Numerical Simulations (DNS) of turbulent flows, and analyze the effect of domain and grid changes. The overall aim is to be familiar with the workings of DNS. Before going into the theory and simulations, this section will give a brief introduction to the characteristics of turbulent flows, for completeness. If you are familiar with turbulent flows, and their characteristics, feel free to skip this section.

Almost every flow we encounter in real life are turbulent, for example waterfall and water in a river. To be able to make good and efficient turbulent applications it is vital to have a good knowledge about turbulent flows. Due to the nature of turbulent flows it is difficult to give a precise definition of them, but they need to have certain characteristics that apply to all of them. If one or more of the characteristics is not met, the particular flow is simply not turbulent. People often think about turbulent flows as just chaotic conditions, but a flow with a chaotic characteristic is not necessarily turbulent.

One of the easiest characteristics to observe is **irregularity**. This means that the turbulent flow structures are random and not repeatable. It is therefore difficult to use a deterministic approach and instead a statistical approach is used. This will be explained in more detail later on. Another characteristic is **diffusivity**. This means that flows transport and mix, and thus spread mass, momentum and heat. Turbulent flows are **rotational, three dimensional and time dependent**. This is easily observed by looking at the vorticity that are created. Turbulent flows have **high Reynolds number**, which means that they have high inertia compared to viscosity. This feature means that the flow has less friction to keep it in order. Turbulent flows also have a **dissipative** characteristic. That means that the high kinetic energy they initially have are dissipated to heat due to viscous stress. To keep the flow going, it needs to get a continued supply of energy. The turbulent characteristics are valid to every fluid, and

thus, turbulence is not a characteristic of the fluid, but rather of the flow.

One of the challenges with turbulent flows is that it is very difficult, if at all possible, to use a deterministic approach to calculate quantities of interest. The most suitable approach is to use a statistical approach. In other words there are no trivial analytic ways to solve turbulent flows, so they have to be solved numerically. To get reasonably good results, this approach demands a lot of computer power. Fortunately the computer power continues to increase these days and the effect of that is that it is feasible to solve them numerically. DNS is one of the computational approaches for turbulent flows and resolve all scales of motion. It is one of the easiest methods conceptually, but one of the most resource demanding methods as well. Because of that it is mostly used in research. More detailed information will be found in the next few chapters.

Part I

RESEARCH METHODOLOGY

 THEORY

This chapter will present the most important theory about turbulent flows. Some important equations will be derived from the basic equations of motion, and then explained extensively. This is done to make it easier to follow and to understand the results produced from the DNS simulations. As explained in the preface, this thesis is a continuation from the project work during the fall of 2017, so most of the theory still apply, and are taken directly from the project work [3]. This is an unpublished project work which can be found at the Department of Energy and Process Engineering at NTNU.

2.1 EQUATIONS OF MOTION

The fundamental governing equations are exactly that, fundamental, and describes the conservation of mass, momentum and energy, and are derived from the principles of physics. They are called continuity, momentum and energy equation, respectively. They are very important tools for the ability to analyze and simulate different fluid flows. They are listed below, in the same order as described above, using Einstein's summation convention. Note that the energy equation (3) is added for completion only, as it is not of interest for the work presented in this thesis.

$$\frac{\partial \rho}{\partial t} + \frac{\partial(\rho u_i)}{\partial x_i} = 0 \quad (1)$$

$$\frac{\partial(\rho u_i)}{\partial t} + \frac{\partial(\rho u_i u_j)}{\partial x_j} = \frac{\partial \sigma_{ij}}{\partial x_j} + \rho f_i \quad (2)$$

$$\frac{\partial(\rho e)}{\partial t} + \frac{\partial(\rho e u_i)}{\partial x_i} = -\frac{\partial(p u_i)}{\partial x_i} + \frac{\partial(\tau_{ij} u_j)}{\partial x_i} + \rho f_i u_i - \frac{\partial(q_i)}{\partial x_i} \quad (3)$$

Here σ_{ij} is the stress tensor, f_i represents gravity and other body forces in i direction, which will not be included going further for simplicity. e is the energy per unit mass,

q_i is the heat flow per unit area and $\tau_{ij} = \mu \left(\frac{\partial u_i}{\partial x_j} + \frac{\partial u_j}{\partial x_i} \right)$ is the viscous stress tensor which is proportional to the rate of deformation. In general the stress tensor is given by

$$\sigma_{ij} = -p\delta_{ij} + \mu \left(\frac{\partial u_i}{\partial x_j} + \frac{\partial u_j}{\partial x_i} - \frac{2}{3}\delta_{ij} \frac{\partial u_k}{\partial x_k} \right) + \mu_B \delta_{ij} \frac{\partial u_k}{\partial x_k}, \quad (4)$$

where μ is dynamic viscosity, also called the first viscosity coefficient, and $\mu_B = \lambda + \frac{2}{3}\mu$ is called the bulk viscosity and describes the energy exchange between translational and internal energy at molecular level [4]. λ is called the second viscosity coefficient. According to Ertesvåg [5], the bulk viscosity is $\mu_B = 0$ which simplifies the equation further. Kronecker delta, δ_{ij} , is defined by

$$\delta_{ij} = \begin{cases} 1 & \text{for } i = j \\ 0 & \text{for } i \neq j \end{cases} \quad (5)$$

As stated earlier the energy equation (3) will not be considered in much detail in this thesis and instead the kinetic energy will be derived and used later to investigate the viscous dissipation of turbulent energy. This thesis will only consider incompressible Newtonian fluid, which will simplify the equations. Equation (1) will then become

$$\frac{\partial u_k}{\partial x_k} = 0, \quad (6)$$

which implies zero volumetric deformation. This simplification can be used in equation (2) to yield the following

$$\rho \left(\frac{\partial u_i}{\partial t} + u_j \frac{\partial u_i}{\partial x_j} \right) = -\frac{\partial p}{\partial x_i} + 2\mu \frac{\partial s_{ij}}{\partial x_j}, \quad (7)$$

where the rate of strain is defined by $s_{ij} = \frac{1}{2} \left(\frac{\partial u_i}{\partial x_j} + \frac{\partial u_j}{\partial x_i} \right)$. The Einstein summation convention is a way to write vector and tensor expressions in a compact way. It uses indices, e.g i , j and k , to represent the dimensions. If an index appears twice in a term, it is called a dummy index and represents a summation over all possible values of that index. ([6], p. 26)

2.2 TURBULENT EQUATIONS OF MOTION

Turbulence consists of random, irregular and unpredictable velocity fluctuations which cannot be solved using a deterministic approach, and has to be statistically modelled. Reynolds [7] assumed that all quantities characterizing the flow could be decomposed into a mean and a fluctuating value. E.g pressure could be expressed as

$$\tilde{p} = P + p \quad (8)$$

where \tilde{p} is the instantaneous value, P is the mean, time averaged, value and p is the fluctuation. P is defined by

$$P = \lim_{T \rightarrow \infty} \frac{1}{T} \int_{t_0}^{t_0+T} \tilde{p} dt. \quad (9)$$

This is of course the ideal case, where the period $T \rightarrow \infty$, but in practice T is finite and is called the "time-window". T must be large compared to the largest turbulence time scale and short compared to the time variations of the mean. The mean value of the fluctuations are zero as can be seen from the following equation

$$\bar{p} = \lim_{T \rightarrow \infty} \frac{1}{T} \int_{t_0}^{t_0+T} (\tilde{p} - P) dt = 0. \quad (10)$$

This means that fluctuations have zero mean. This holds true also for velocity and the stress tensor. The use of an overbar on fluctuations means the mean value of that quantity.

2.2.1 REYNOLDS DECOMPOSITION

Using the same convention as in equation (8) the equations of motion then becomes

$$\frac{\partial \tilde{u}_i}{\partial x_i} = 0, \quad (11)$$

$$\frac{\partial \tilde{u}_i}{\partial t} + \tilde{u}_j \frac{\partial \tilde{u}_i}{\partial x_j} = \frac{1}{\rho} \frac{\partial \tilde{\sigma}_{ij}}{\partial x_j}. \quad (12)$$

Equations (11) and (12) are continuity equation and momentum equation respectively. In an incompressible Newtonian fluid the stress tensor, $\tilde{\sigma}_{ij}$, is given by

$$\tilde{\sigma}_{ij} = -\tilde{p}\delta_{ij} + 2\mu\tilde{s}_{ij}, \quad (13)$$

which means that it accounts for both pressure and viscous stresses. By combining the equations above the equation below is obtained:

$$\frac{\partial \tilde{u}_i}{\partial t} + \tilde{u}_j \frac{\partial \tilde{u}_i}{\partial x_j} = -\frac{1}{\rho} \frac{\partial \tilde{p}}{\partial x_i} + \nu \frac{\partial^2 \tilde{u}_i}{\partial x_j \partial x_j}. \quad (14)$$

Here, $\nu = \frac{\mu}{\rho}$ is the kinematic viscosity. Before applying the Reynolds decomposition on equations (11) and (12) there are some rules that need to be established. For two signals $\tilde{a} = A + a$ and $\tilde{b} = B + b$ then the following rules apply:

$$\overline{\tilde{a} + \tilde{b}} = A + B \quad \overline{A \cdot B} = A \cdot B \quad \overline{A b} = 0 \quad \overline{b A} = 0 \quad \overline{a B} = A \cdot B \quad \overline{\tilde{a} \tilde{b}} = A \cdot B + \overline{a b}. \quad (15)$$

2.2.2 EQUATIONS FOR THE MEAN FLOW

If equation (11) now is expanded using Reynolds decomposition and then take the average, the following will be obtained, respectively:

$$\frac{\partial \tilde{u}_i}{\partial x_i} = \frac{\partial}{\partial x_i} (U_i + u_i) = \frac{\partial U_i}{\partial x_i} + \frac{\partial u_i}{\partial x_i} = 0 \quad (16)$$

and

$$\frac{\partial \overline{\tilde{u}_i}}{\partial x_i} = \frac{\partial}{\partial x_i} \overline{(U_i + u_i)} = \frac{\partial U_i}{\partial x_i} + \frac{\partial \overline{u_i}}{\partial x_i} = 0. \quad (17)$$

Here $\frac{\partial \overline{u_i}}{\partial x_i} = 0$ because of the rule in equation (10). This leads to $\frac{\partial U_i}{\partial x_i} = 0$ and according to equation (16), $\frac{\partial u_i}{\partial x_i} = 0$. This means that both the mean and fluctuating velocity independently satisfy mass conservation.

Using Reynolds decomposition again on equation (12), applying the rules given in equation (15) and taking the average this yields

$$\frac{\partial U_i}{\partial t} + U_j \frac{\partial U_i}{\partial x_j} = \frac{1}{\rho} \frac{\partial}{\partial x_j} \Sigma_{ij} - \overline{u_j \frac{\partial u_i}{\partial x_j}}, \quad (18)$$

where $\Sigma_{ij} = -P\delta_{ij} + 2\mu S_{ij}$ is called the mean stress tensor. Using the chain rule in differentiation, it can be shown that $\overline{u_j \frac{\partial u_i}{\partial x_j}} = \frac{\partial}{\partial x_j} \overline{(u_i u_j)} - \overline{u_i \frac{\partial u_j}{\partial x_j}}$, where the last term on the right hand side is zero due to continuity equation. By putting this into equation (18) the Reynolds-averaged Navier-Stokes (RANS) equation will be obtained. It is given by

$$\frac{\partial U_i}{\partial t} + U_j \frac{\partial U_i}{\partial x_j} = \frac{1}{\rho} \frac{\partial}{\partial x_j} (\Sigma_{ij} - \rho \overline{u_i u_j}). \quad (19)$$

As can easily be seen, RANS is an equation for the mean velocity U_i and mean pressure P . Equation (19) is almost the same as Navier-Stokes for laminar flows except for the new term $\rho \overline{u_i u_j}$ which is totally unknown and represents turbulent transport of momentum. It looks like a stress tensor similarly as Σ_{ij} and the interpretation of this is that turbulence has an effect on the mean flow which is the production of extra stresses. The turbulent stresses, also called Reynolds stresses, are denoted $\tau_{ij} = -\rho \overline{u_i u_j}$ and originate from the non-linear term in the momentum equation and are therefore a property of the flow. This is not the same τ_{ij} as the one shown in equation (3). The total mean stress tensor in turbulence is

$$T_{ij} = -P\delta_{ij} + 2\mu S_{ij} - \rho \overline{u_i u_j}, \quad (20)$$

which is the sum of the stress tensor in the mean flow and the turbulent stresses, and consists of pressure, viscous and turbulent stresses. By decomposing the flow into a

mean and a fluctuating part it has become easier to differentiate the effects of turbulence on the mean flow.

In order to be able to investigate how the mean flow affects the turbulence, and how the energy is distributed in turbulence, it is necessary to develop a relation between the energy and the mean flow. This relation is obtained using the term $\frac{1}{2}U_i U_i$, which is called the kinetic energy of the mean flow. By multiplying U_i with equation (19) and summing over i -indices the energy equation is obtained ([8], p. 60):

$$\rho \left[\frac{\partial K}{\partial t} + U_j \frac{\partial K}{\partial x_j} \right] = \frac{\partial}{\partial x_j} (T_{ij} U_i) - T_{ij} \frac{\partial U_i}{\partial x_j}, \quad (21)$$

where $K = \frac{1}{2}U_i U_i$. Here, the chain rule is used in order to divide the stress term into two terms. That makes it easier to make a physical interpretation. The second term on the left hand side of equation (21) represents the variation of kinetic energy due to advection. The first term on the right hand side represents energy transport of the mean flow caused by total mean stress, T_{ij} , and the second term represents deformation work of the fluid element. The kinetic energy changes due to gain or loss caused by the deformation work. To better view the effects of viscosity equation (20) is substituted into (21) and then the energy equation for the mean flow becomes

$$\rho \left[\frac{\partial K}{\partial t} + U_j \frac{\partial K}{\partial x_j} \right] = \frac{\partial}{\partial x_j} (-P \delta_{ij} U_i + 2\mu S_{ij} U_i - \rho \overline{u_i u_j} U_i) - 2\mu S_{ij} S_{ij} + \rho \overline{u_i u_j} S_{ij}. \quad (22)$$

Here, the first term on the right hand side is the pressure work, the second term is energy transport by viscous stresses and the third is energy transport by turbulent stresses. The fourth term is viscous deformation work and the last term is turbulent deformation work. Because most turbulent flows have a high Reynolds number the viscous terms can be neglected, except very close to walls or other smooth surfaces. Viscous deformation work represents loss of kinetic energy and is therefore negative. The term $2\mu S_{ij} S_{ij}$ is called viscous dissipation. The last term is usually negative, but can be positive locally in the flow. This term is known as turbulent energy production because the loss of mean flow energy is transferred to the turbulent fluctuations, and the turbulent kinetic energy increases. This will be addressed later in this thesis.

Because the energy equation of the mean flow is obtained by mathematical manipulation of the momentum equation for the mean flow, the energy equation does not contain any more information than the momentum equation ([8], p. 63). Now it is interesting to look at the equation for the turbulent kinetic energy, $k = \frac{1}{2}\overline{u_i u_i}$ which will be covered in the next section.

2.2.3 EQUATIONS FOR THE TURBULENT FLUCTUATIONS

By multiplying equation (12) by \tilde{u}_i , taking the time average and then subtract equation (22), the kinetic energy of turbulence is obtained ([8], p. 63). The equation is as follows

$$\frac{\partial k}{\partial t} + U_j \frac{\partial k}{\partial x_j} = -\frac{\partial}{\partial x_j} \left[\frac{1}{\rho} \overline{u_j p} + \frac{1}{2} \overline{u_i u_i u_j} - 2\nu \overline{u_i s_{ij}} \right] - \overline{u_i u_j} S_{ij} - 2\nu \overline{s_{ij} s_{ij}}, \quad (23)$$

where $k = \frac{1}{2} \overline{u_i u_i}$ is the mean kinetic energy of the turbulent velocity fluctuations. Here, s_{ij} is the fluctuating rate of strain and is defined by

$$s_{ij} = \frac{1}{2} \left(\frac{\partial u_i}{\partial x_j} + \frac{\partial u_j}{\partial x_i} \right). \quad (24)$$

The left hand side is the usual rate of change of turbulent kinetic energy. The first two terms on the right hand side represent transport of turbulent energy caused by turbulence. The next term is transport of turbulent energy by means of viscous stresses, while the last two terms are deformation work by turbulent and viscous stresses respectively. The production term $-\overline{u_i u_j} S_{ij}$ is also in equation (22) but with an opposite sign, and is exchanging kinetic energy between the mean flow and the turbulence, and usually the energy is transferring from the mean flow to the turbulence/fluctuations. The last term represents drain of energy due to viscous stresses, also called viscous dissipation. Viscous stresses convert kinetic energy to heat. Viscous dissipation will be analyzed more later on when discussing the results obtained.

In most shear flows the production and dissipation terms are of the same order of magnitude. For example in a steady, homogeneous and pure shear flow, equation (23) reduces to

$$-\overline{u_i u_j} S_{ij} = 2\nu \overline{s_{ij} s_{ij}}. \quad (25)$$

To understand the features of turbulence that are not directly related to spatial transport, equation (25) can be used as an aid. If production is defined as $P_{prod} = -\overline{u_i u_j} S_{ij}$ and the viscous dissipation is defined as $\epsilon = 2\nu \overline{s_{ij} s_{ij}}$ then equation (25) reads $P_{prod} = \epsilon$. If using the scale relations $S_{ij} \sim u/l$ and $-\overline{u_i u_j} \sim u^2$ it can be shown that $ulS_{ij}S_{ij} = 2\nu \overline{s_{ij} s_{ij}}$ ([8], p. 65). Since the Reynolds number, ul/ν , is large in turbulence it can be seen that

$$\overline{s_{ij} s_{ij}} \gg S_{ij} S_{ij}. \quad (26)$$

The equation above means that the fluctuating strain rate is much larger than the mean strain rate. The strain rate has dimensions s^{-1} , and that means that the higher the strain rate the lower the time scale. This means that s_{ij} and S_{ij} do not interact very much because the fluctuating strain rate is much bigger than the mean strain

rate. Because of that, the structure of the small scale turbulence seems to be independent of any orientation caused by the mean shear. The small scale structure is called isotropic if such behavior is present.

2.2.4 VISCOSITY AND DISSIPATION

A convenient way of writing equation (23) is as follows ([5], p.49)

$$\underbrace{\frac{\partial}{\partial t}(\rho k) + \frac{\partial}{\partial x_j}(\rho k U_j)}_{\rho C_k} = \underbrace{-\rho \overline{u_i u_j} \frac{\partial U_i}{\partial x_j}}_{\rho P_k} + \underbrace{\frac{\partial}{\partial x_j} \left(\mu \frac{\partial k}{\partial x_j} \right)}_{\rho D_{k,v}} + \underbrace{\frac{\partial}{\partial x_j} \left(-\frac{1}{2} \rho \overline{u_i u_i u_j} - \overline{\rho u_j} \right)}_{\rho D_{k,t}} - \underbrace{\mu \frac{\partial u_i}{\partial x_j} \frac{\partial u_i}{\partial x_j}}_{\rho \epsilon'} \quad (27)$$

Here, P_k represents the production of energy, $D_{k,v}$ is viscous diffusion, $D_{k,t}$ is turbulent diffusion and lastly ϵ' represents a part of the dissipation. As stated earlier the dissipation, ϵ , is defined by $\epsilon = 2\nu \overline{s_{ij} s_{ij}}$. By expanding the right hand side we get

$$\epsilon = 2\nu \overline{s_{ij} s_{ij}} = 2\nu \overline{\frac{1}{2} \left(\frac{\partial u_i}{\partial x_j} + \frac{\partial u_j}{\partial x_i} \right) \frac{1}{2} \left(\frac{\partial u_i}{\partial x_j} + \frac{\partial u_j}{\partial x_i} \right)} = \nu \overline{\left(\frac{\partial u_i}{\partial x_j} + \frac{\partial u_j}{\partial x_i} \right) \frac{\partial u_i}{\partial x_j}}, \quad (28)$$

where the symmetry $s_{ij} = s_{ji}$ has been used. The dissipation term has been divided into two parts and put into $\rho D_{k,v}$ and $\rho \epsilon'$. This is done for the purpose of having a gradient term for diffusion. Even though they have been divided into two parts, ϵ' contains most of the dissipation and is therefore often referred to as the dissipation. While this is not entirely true, it is commonly used. In homogeneous turbulence, statistically independent of location in space, it can be shown that the dissipation is simplified to ϵ' [9].

2.3 REYNOLDS STRESS

An equation for turbulent stresses, Reynolds stresses, can be derived by the same principles as for the turbulent kinetic energy. By using the Reynolds decomposition on equation (12), get an expression for $\frac{\partial u}{\partial t}$ for both i and j directions, use the chain rule on the expression for the Reynolds stresses, $\frac{\partial}{\partial t}(u_i u_j) = u_j \frac{\partial u_i}{\partial t} + u_i \frac{\partial u_j}{\partial t}$, and then take the average the equation for Reynolds stresses the following is obtained ([5], p.95):

$$\begin{aligned}
\underbrace{\frac{\partial}{\partial t}(\rho \overline{u_i u_j}) + \frac{\partial}{\partial x_k}(\rho \overline{u_i u_j} U_k)}_{\rho C_{ij}} &= - \underbrace{\left(\rho \overline{u_i u_k} \frac{\partial U_j}{\partial x_k} + \rho \overline{u_j u_k} \frac{\partial U_i}{\partial x_k} \right)}_{\rho P_{ij}} + \underbrace{\frac{\partial}{\partial x_k} \left(\mu \frac{\partial \overline{u_i u_j}}{\partial x_k} \right)}_{\rho D_{ij,v}} \\
&+ \underbrace{\frac{\partial}{\partial x_k} (-\rho \overline{u_i u_j} u_k - (\overline{p u_i} \delta_{jk} + \overline{p u_j} \delta_{ik}))}_{\rho D_{ij,t}} \\
&+ \underbrace{p \left(\frac{\partial u_i}{\partial x_j} + \frac{\partial u_j}{\partial x_i} \right)}_{\rho \phi_{ij}} - \underbrace{2\mu \frac{\partial u_i}{\partial x_k} \frac{\partial u_j}{\partial x_k}}_{\rho \epsilon_{ij}}.
\end{aligned} \tag{29}$$

The terms in the equation above have mostly the same purpose as those in equation (27), with the difference that they are done by the Reynolds stresses. P_{ij} is the production of kinetic energy from the mean flow to the turbulent flow. $D_{ij,v}$ is the viscous diffusion and $D_{ij,t}$ is the turbulent diffusion. ϕ_{ij} is energy that is exchanged between the other components and is neither lost nor produced, just redistributed in the flow. The last term expresses dissipation due to viscosity in the Reynolds stress. This energy is lost through heat. It can be shown, by comparing ϵ_{ij} to ϵ' in equations (29) and (27) respectively, that $\epsilon_{11} + \epsilon_{22} + \epsilon_{33} = 2\epsilon'$. This can be shown mathematically by using the Kronecker delta operator, δ_{ij} , as follows

$$2\mu \frac{\partial u_i}{\partial x_k} \frac{\partial u_j}{\partial x_k} \delta_{ij} = 2\mu \frac{\partial u_i}{\partial x_k} \frac{\partial u_i}{\partial x_k}. \tag{30}$$

The next section will address how the energy will flow from the mean flow to the turbulence and from larger scales to smaller ones, and the break-ups of scales from larger scales to smaller ones.

2.4 TURBULENT SCALES AND ENERGY CONVERSION

Now that the equations of turbulent motion and kinetic energy are established it is time to go into how the energy is transferred in the turbulent flow. In a turbulent flow the energy is produced and transferred from the mean flow to the turbulent fluctuations and from there, in the end, lost by viscous dissipation. Before going into the energy transformation the turbulent scales are briefly discussed.

In turbulent motion the length scale is a quantity that relates the motion to a physical size. Going further in the explanations the turbulent flow is considered to have a high Reynolds number, a length scale \mathcal{L} and a characteristic velocity \mathcal{U} . Richardson

[10] introduced the energy cascade concept and characterized turbulence as a hierarchy of scales and considered turbulent motion to consist of eddies of different size. There is no clear and precise definition of an eddy, but it can be understood as any kind of turbulent motion ([2] p. 183). The length, velocity and time scales of eddies are denoted ℓ , $u(\ell)$ and $\tau = \frac{\ell}{u(\ell)}$, respectively. At the beginning of the energy cascade the largest eddies exist with high kinetic energy which is then transferred to smaller and smaller scales. The Reynolds number is here very large and therefore the viscosity is not of importance. At sufficiently small scales the Reynolds number becomes small enough so that viscosity does play an important role and creates a stable eddy motion until the energy is dissipated by the viscosity. This is the end of the energy cascade. The reason for the break up of larger scales to smaller ones is, according to Richardson, that the large eddies are unstable and then break up.

The largest eddies have a length scale ℓ_0 , characteristic velocity $u(\ell_0)$ and time scale τ_0 . The first two are considered to be in the same order as the flow scale \mathcal{L} and \mathcal{U} respectively, which means that they have approximately the same Reynolds number, which is large, and therefore the viscous effects are small. The Russian mathematician Andrey Kolmogorov had a big influence on the development of turbulence, as will be discussed further on. According to Kolmogorov's hypothesis of local isotropy, in flows at high enough Reynolds number the smaller scales will gradually be less dependent on directions, i.e the directional information will be lost when $\ell \ll \ell_0$ ([2] p. 184). This is called isotropic turbulence. The consequence of this is that both the characteristic velocity and time scale decreases as ℓ decreases. As the scales becomes smaller and smaller the Reynolds number will decrease, which means that viscous effects will be greater. Kolmogorov assumed that since the directional information is lost the geometry and boundary conditions are also lost. This makes the directional and boundary condition information for small enough eddies to be the same. This leads to Kolmogorov's first similarity hypothesis, which states: "In every turbulent flow at sufficiently high Reynolds number, the statistics of the small-scale motions have a universal form that is uniquely determined by ν and ϵ " ([2], p. 185). This assumption implies that the smaller eddies are determined only by the energy dissipation rate, ϵ , and the kinematic viscosity, ν . Kolmogorov defined equations for the small scale which are the following:

$$\eta \equiv (\nu^3/\epsilon)^{1/4}, \quad (31)$$

$$u_\eta \equiv (\epsilon\nu)^{1/4} \quad (32)$$

and

$$\tau_\eta \equiv (\nu/\epsilon)^{1/2}. \quad (33)$$

Here, $\ell = \eta$ is the length scale for the small scale eddies. u_η and τ_η represents the small scale velocity and time respectively. As can be seen from Kolmogorov's mi-

crosscales is that the Reynolds number is equal to one. This means that viscosity cannot be neglected. The break up of eddies will stop at this length scale and viscosity will convert the kinetic energy to heat. The kinetic energy per mass of the large eddies are of the order u_0^2 and by dimensional analysis it can be shown that $\epsilon \sim u_0^3/\ell_0$. By combining these relations the comparison between the integral scales (large scale motion) and the kolmogorov scales can be obtained.

$$\frac{\eta}{\ell_0} = \left(\frac{u_0 \ell_0}{\nu} \right)^{-3/4} = Re^{-3/4} \quad (34)$$

$$\frac{u_\eta}{u_0} = Re^{-1/4} \quad (35)$$

$$\frac{\tau_\eta}{\tau_0} = Re^{-1/2} \quad (36)$$

From this we can see that increasing Reynolds number decreases the small scale to integral scale ratios.

2.5 PIONEERING ARTICLE BY KIM ET AL.(1987)

Kim et al.[1] wrote a pioneering article in 1987 about a performed Direct Numerical Simulation of a fully developed channel flow at low Reynolds number. The work published in this article often works as a reference when performing a DNS of a channel flow and is considered to be very accurate. This section will give a brief summary of the most relevant information from this article.

The objective of the article was to perform a DNS where all essential scales of motion are solved. The performed DNS was done solving the unsteady Navier-Stokes equations numerically at a Reynolds number of 3300, which was based on the mean centreline velocity and the half-width of the channel δ , with $Re_\tau = 180$, which is the Reynolds number based on the wall shear velocity u_τ . The grid resolution used was $192 \times 160 \times 129$, in x, y and z, resulting in 3 962 880 grid points. Here x, y and z are streamwise, spanwise and wall-normal directions respectively, which is different from what is used in Kim et al.[1], but reflects the convention used in this thesis. The domain size is $4\pi\delta$ in streamwise direction, $2\pi\delta$ in spanwise direction and 2δ in wall-normal direction. The grid spacing are $\Delta x^+ = \frac{4\pi}{192} \cdot 180 \approx 12$ and $\Delta y^+ = \frac{2\pi}{160} \cdot 180 \approx 7$ in streamwise and spanwise direction respectively. They used two-point correlations and energy spectra to make sure that both the domain size and grid resolution were adequate.

The numerical approach used in this article is a little different than what was used in this thesis. For the spatial derivatives a spectral method is used. For the streamwise and spanwise, the homogeneous directions, Fourier series are used. For the

wall-normal direction the Chebychev polynomial expansion is used. The temporal discretization is performed using Crank-Nicholson for the viscous terms and Adams-Bashforth for the non-linear terms, which are semi-implicit schemes. They compare the results against other experiments at comparably low Reynolds numbers and discuss the discrepancies. The characteristics of the turbulence statistics correspond well in general with the experimental results, but clearly have some discrepancies, especially close to the wall. They mention that the measurement of u_τ may be one of the reasons for the discrepancy. When the mean velocity profiles are re-normalized with the experimental u_τ it seems to better correspond with the experimental results. The same happens when the turbulence intensities and Reynolds shear stress are re-normalized with the same u_τ .

FLOW DOMAIN AND GEOMETRY

As described in the problem formulation multiple DNS simulations have been performed with different grid resolutions and flow domain sizes. The flow geometry is a channel flow as shown in Figure (1). Here x , y and z denotes the streamwise, spanwise and wall normal directions, respectively. This chapter will provide basic theory about channel flows.

3.1 CHANNEL FLOW

A fully developed turbulent channel flow has been simulated using Direct Numerical Simulations (DNS). This geometry has often been chosen due to its simplicity to do experiments of turbulent flows near a wall, where a lot of the complexity is happening.

Figure (1) shows the channel geometry, where the streamwise and spanwise directions are homogeneous due to the fact that it is a fully developed flow. More information about the simulations will be given in the next several chapters. The length, width and height are denoted l_x , l_y and l_z , respectively.

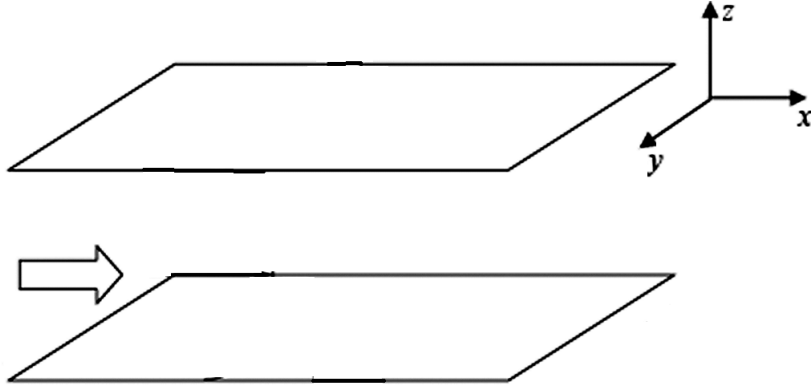


Figure 1: Geometry and coordinate system of the flow

3.2 FLOW ALONG A SOLID SURFACE

To get a grasp of the theory behind flows through a fully developed channel flow it seems to be a good idea to introduce some important parameters and definitions especially near the wall. The no-slip and impermeability conditions hold true at the wall, which means that $\tilde{u}_i = 0$, where \tilde{u}_i is the instantaneous velocity. No-slip condition means that the velocity along the wall is zero and the impermeability condition means that the flow cannot go through the wall and the velocity is therefore zero perpendicular to the wall. At the solid wall the turbulence is damped out, which means that $\tau_{ij} = -\rho \overline{u_i u_j} = 0$. The flow has a zero mean spanwise velocity, $V = 0$. Since the flow is fully developed the velocity statistics are only dependent on z . From this it follows that $\frac{dU}{dx} = 0$. The continuity equation then reduces to $\frac{dW}{dz} = 0$. From the impermeability condition, $W_{wall} = 0$, this results in $W = 0$ for all z . The total mean shear stress is therefore given by

$$T_{ij} = \rho \nu \frac{dU}{dz} - \rho \overline{u_i u_j}, \quad (37)$$

where $i \neq j$. $\overline{u_i u_j}$ and $\overline{v_i v_j}$ are zero. Since the Reynolds stresses are zero at the wall, the wall mean shear stress becomes

$$T_w \equiv \rho \nu \left(\frac{dU}{dz} \right)_{y=0}, \quad (38)$$

which indicates that the wall mean shear stress is due to viscosity only. To get more detailed information the reader is recommended to take a look at ([2], p. 269). Since much of the complexity, and thus the most interesting things, are happening near

the wall, parameters used in that region would benefit from having a new scale that represents the region. First the friction velocity, or shear stress velocity, is defined as

$$u_\tau \equiv \sqrt{\frac{T_w}{\rho}}, \quad (39)$$

and the viscous length scale can be defined by

$$\delta_\nu \equiv \nu \sqrt{\frac{\rho}{\tau_w}} = \frac{\nu}{u_\tau}. \quad (40)$$

By using the two scales above, the friction Reynolds number can be defined as follows

$$Re_\tau \equiv \frac{u_\tau l_z}{\nu}. \quad (41)$$

Near the wall it is assumed that the mean velocity only depends on u_τ , z and ν as follows

$$U = f(u_\tau, z, \nu), \quad (42)$$

and we can define a new parameter u^+ , which is the mean velocity normalized by the friction velocity, as a function of another new parameter z^+ as follows

$$u^+ = f(z^+). \quad (43)$$

z^+ is defined as $z^+ \equiv \frac{u_\tau z}{\nu}$ and indicates a wall distance following the viscous length scale. Equation (43) is called "law of the wall" and says that the normalized velocity is a function of the wall distance. The normalized velocity is defined by

$$u^+ \equiv \frac{U}{u_\tau}. \quad (44)$$

As stated earlier, close to the wall the Reynolds shear stress is small compared to viscous stress, so the total mean shear stress can be approximated as

$$T_{xz} \approx \rho u_\tau^2, \quad (45)$$

which means that we can assume the following, close to the wall:

$$\mu \frac{dU}{dz} = \rho u_\tau^2, \quad (46)$$

and when solved for U this gives

$$U = \frac{u_\tau^2}{\nu} z + \text{constant}. \quad (47)$$

By setting the constant to zero and rearranging the equation we get the following

$$u^+ = z^+. \quad (48)$$

By going further out, viscosity becomes smaller and at some point it can be neglected as is clear by the fact that z^+ is getting bigger. This will be further discussed later. By doing some dimensional analysis it can be shown that $\frac{dU}{dz} = \frac{1}{\kappa} \frac{u_\tau}{z}$ [11] [Andersson, H. I., Lecture Notes, February 7, 2017]. By integration and further mathematical manipulation this becomes

$$u^+ = \frac{1}{\kappa} \ln z^+ + A, \quad (49)$$

where A is a constant set to 5.5 here. This has empirically been proven to be correct. Equation (49) is called the logarithmic law of the wall, or just the log law. κ is called the von Kármán constant, set to 0.4, after Theodor von Kármán ([2], p. 274). It is common to divide different values of z^+ into layers, the inner layer and the outer layer, and for each layer again divide into sublayers. In Table (1), reproduced from ([2], p. 275), a description of the different layers can be found. In Figure (2) the different layers are shown, divided into $z^+ = 5$, $z^+ = 30$ and $z^+ = 50$. The data used in Figure (2) are extracted from [12], which is a database consisting of data from [1]. The data seems to correspond well with Table (1). The plot for equation (48) clearly fits well with the data from [12] for $z^+ < 5$ and for z^+ between 30 and 50 it fits clearly with equation (49).

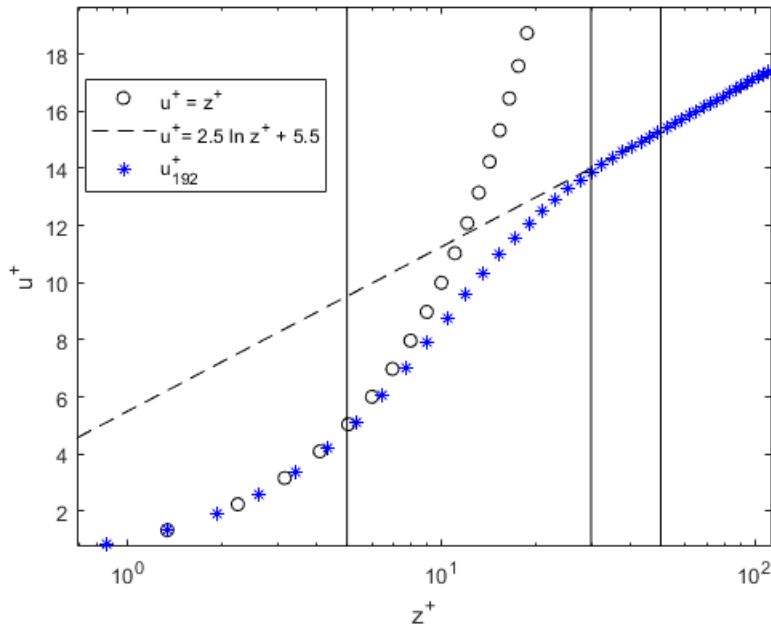


Figure 2: u_{192}^+ plotted against different wall region layers in $\log z^+$.

Region	Location	Defining property
Inner layer	z/δ	U determined by u_τ and z^+
Viscous wall region	$z^+ < 50$	Significant contribution from viscosity to shear stress
Viscous sublayer	$z^+ < 5$	Reynolds shear stress is negligible compared with the viscous stress
Outer layer	$z^+ > 50$	Direct effects of viscosity on U are negligible
Overlap region	$z^+ > 50, z/\delta < 0.1$	Region of overlap between inner and outer layers
Log-law region	$z^+ > 30, z/\delta < 0.3$	The log-law holds
Buffer layer	$5 < z^+ < 30$	The region between the viscous sublayer and the log-law region

Table 1: Wall region layers ([2], p. 275)

NUMERICAL SOLUTIONS

The source code used for the simulations originated from Delft University of Technology in the Netherlands and was written in the programming language Fortran by Professor Boersma and Dr. Gillisen. It uses parallelization using Message Passing Interface (MPI). The code has been used several times and has been verified and validated. The subsequent sections briefly present the most important equations and numerical algorithms used in the DNS code.

4.1 DIRECT NUMERICAL SIMULATION

The ultimate objective of using a DNS is to resolve all scales of motion in turbulent flows and this is done by solving the Navier-Stokes equations (2). The number of grid points is determined by the product of the number of grid points in each of the three directions: $N_{tot} = N_x N_y N_z$. The process of solving equation (2) takes a lot of computing power and according to ([13], p. 307) the time steps grows with $Re^{1/2}$ and the number of grid points grows with $Re^{3/4}$, which gives a total of $Re^{11/4}$. Because the computer power increases so fast with Reynolds number, it limits the use of DNS to low Reynolds numbers.

4.2 EQUATIONS SOLVED

The equations used to solve the turbulent channel flow is the non-dimensionalized Navier-Stokes equation, or momentum equation, (2). The friction Reynolds number is $Re_\tau = 360$, which is based on the channel height. To get the non-dimensionalized momentum equation the non-dimensionalized variables are used. They are indicated by a star, as follows

$$x^* = \frac{x}{l_z} \quad \vec{u}^* = \frac{\vec{u}}{u_\tau} \quad t^* = \frac{t u_\tau}{l_z} \quad p^* = \frac{p}{\rho u_\tau^2}. \quad (50)$$

By inserting these into equation (2) and mathematically manipulate it, the non-dimensionalized continuity and momentum equation becomes [14]

$$\frac{\partial u_i^*}{\partial x_i^*} = 0 \quad (51)$$

$$\frac{\partial u_i^*}{\partial t^*} + \frac{\partial u_i^* u_j^*}{\partial x_j^*} = -\frac{\partial p^*}{\partial x_i^*} + \frac{1}{Re_\tau} \frac{\partial^2 u_i^*}{\partial x_j^* \partial x_j^*}. \quad (52)$$

4.3 PRESSURE-VELOCITY COUPLING

The Navier-Stokes equations are a set of equations for velocity and pressure (pressure gradient), and represents the momentum equation in x, y and z directions. What makes this difficult to solve is the fact that it does not have an independent equation for the pressure for the three directional momentum equations. For incompressible flows, the continuity equation does not have a dominant variable and it cannot be used to calculate the pressure, as opposed to compressible flows. One solution is to make sure that pressure at each time step is constructed in such a way to fulfill the conservation of mass. This can be solved by a multiple of different types of schemes such as Explicit Time Advance Scheme and Implicit Time Advance Method. The method used here is a projection method, and satisfies the conservation of mass ([15], p. 167). The next sections will briefly go into what discretization schemes that are used in this DNS code.

4.4 DISCRETIZATION SCHEMES

Navier-Stokes equations are Partial Differential Equations (PDE) and are impossible to solve analytically, except in some special cases. They have to be numerically solved. This suggests that an approximate solution needs to be obtained. This is done by using a discretization scheme. This section will provide information about the discretization schemes used, both in space and in time. The streamwise and spanwise directions are, as stated in Chapter (3), homogeneous and have a uniform grid. The wall normal direction has a non-uniform staggered grid, as shown in Figure (3). The filled and unfilled circles here represent the cell centers and cell faces respectively. The positions on the cell faces are represented by z_i^F and go from $i = 0$ to $i = N$, where $z_0^F = 0$ and $z_N^F = 1$. It is easily seen that Δz_i^F increases further away from the walls, and thus are non-uniform. It is stretched to give finer resolution close to the wall. This is necessary because close to the wall is where the complexity is happening

and is thus more important than further away. The positions of the cell faces and cell centers in z direction are found by the following equations, respectively.

$$z_i^F(k, s) = \frac{1}{2} \frac{\tan^{-1}(sk - \frac{1}{2}s)}{\tan^{-1}(\frac{1}{2}s)} + \frac{1}{2}, \quad k = 0, \frac{1}{N_z}, \frac{2}{N_z}, \dots, 1 \quad (53)$$

$$z_i^C = (z_i^F + z_{i-1}^F)/2. \quad (54)$$

Here s is the stretching factor. The spatial derivatives in the homogeneous directions are solved using a pseudo-spectral method. The spatial derivatives and velocities in the homogeneous directions, u and v , are calculated at the cell centers, which also is the case for the pressure. The spatial derivatives in the wall-normal direction are computed using a second-order, central finite difference scheme. The spatial derivatives and velocity for the wall-normal direction is calculated at the cell faces. For the time advancement, a second-order, explicit Adams-Bashforth (AB2) scheme is used. [16]

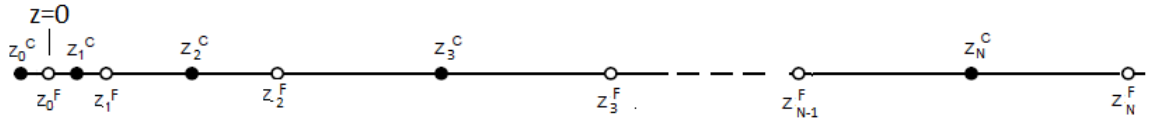


Figure 3: Discretized grid in wall normal direction. The black filled circles represent the cell centers, while the unfilled circles represent the cell faces.

4.4.1 SPATIAL DERIVATIVES IN HOMOGENEOUS DIRECTIONS

The spatial derivatives in the homogeneous directions are computed using the pseudo-spectral method, which means that the variables are transformed into wavenumber space. The transformations are done with Fast Fourier Transform (FFT). After completing the calculations the variables are then transformed back to physical space using the inverse FFT (FFT^{-1}).

Let $u(x_j)$ be a periodic function in x direction that is discretized on a domain with period/length l_x and N_x grid points. Then $\Delta x = \frac{l_x}{N_x}$ is the sample length. The discrete sampling location is $x_j = j \frac{l_x}{N_x}$, where j is an integer. The complex coefficient of the Fourier transform are given by the following equation.

$$\hat{u} = \frac{1}{N_x} \sum_{j=0}^{N_x-1} u(x_j) e^{-\frac{2\pi}{l_x} k x_j}, \quad k = -\frac{N_x}{2}, \dots, \frac{N_x}{2} - 1 \quad (55)$$

where k is the wavenumber. The complex Fourier coefficients is represented by the following equation and are calculated by the FFT algorithm. [16]

$$u(x_j) = \sum_{k=-\frac{N_x}{2}}^{\frac{N_x}{2}-1} \hat{u}(x_j) e^{\frac{2\pi i k}{l_x} x_j}, \quad j = 0, \dots, N_x - 1 \quad (56)$$

where j is in the range $0 \leq k \leq N_x - 1$. For more detailed information take a look at Pope [2], p. 670-695. An advantage of using the Fourier transform is that the derivative is simply just a matter of multiplication. This makes it fast and efficient. The formula for the derivative is the following.

$$\frac{d^n u(x)}{dx^n} = \mathcal{F}^{-1}\{(i\omega)^n \mathcal{F}\{u(x)\}\}, \quad (57)$$

where $\omega = \frac{2\pi k}{l_x}$ is the frequency. The first and second-order derivative are given by the equations below, respectively.

$$\frac{du(x_j)}{dx} = \sum_{k=-\frac{N_x}{2}}^{\frac{N_x}{2}-1} \frac{2\pi i k}{l_x} \hat{u} e^{\frac{2\pi i k}{l_x} x_j}, \quad j = 0, \dots, N_x - 1 \quad (58)$$

$$\frac{d^2 u(x_j)}{dx^2} = \sum_{k=-\frac{N_x}{2}}^{\frac{N_x}{2}-1} -\left(\frac{2\pi i k}{l_x}\right)^2 \hat{u} e^{\frac{2\pi i k}{l_x} x_j}, \quad j = 0, \dots, N_x - 1 \quad (59)$$

4.4.2 SPATIAL DERIVATIVES IN WALL-NORMAL DIRECTION

In wall-normal direction, second-order central differencing schemes are used to compute the derivatives. On a non-uniform grid this gives a first-order accuracy. As before, the indices F and C indicates cell face and cell centers, respectively. The first-order derivatives for cell face and cell centers are computed as follows, respectively.

$$\frac{d}{dz} u_j^C = \frac{u_j^F - u_{j-1}^F}{z_j^F - z_{j-1}^F}, \quad (60)$$

$$\frac{d}{dz} u_j^F = \frac{u_{j+1}^C - u_j^C}{z_{j+1}^C - z_j^C}, \quad (61)$$

where z_j indicates the sampling location at grid cell j . For the second-order derivatives, the following equations are used.

$$\frac{d^2}{dz^2} u_j^C = \frac{\frac{u_{j+1}^C - u_j^C}{z_{j+1}^C - z_j^C} - \frac{u_j^C - u_{j-1}^C}{z_j^C - z_{j-1}^C}}{z_j^F - z_{j-1}^F}, \quad (62)$$

$$\frac{d^2}{dz^2} u_j^F = \frac{\frac{u_{j+1}^F - u_j^F}{z_{j+1}^F - z_j^F} - \frac{u_j^F - u_{j-1}^F}{z_j^F - z_{j-1}^F}}{z_{j+1}^C - z_j^C}. \quad (63)$$

Sometimes it is convenient to calculate quantities at cell faces and cell centers when only one is known. An interpolating scheme is used to calculate one from the other, shown below.

$$u_j^F = \frac{u_{j+1}^C + u_j^C}{2}, \quad (64)$$

$$u_j^C = \frac{u_j^F + u_{j-1}^F}{2}. \quad (65)$$

4.4.3 TEMPORAL DISCRETIZATION

The two previous sections have talked about discretization of the Navier-Stokes equations in space. This section will talk about how the equations are discretized and stepped forward in time. A second-order Adams-Bashforth scheme is used for temporal discretization, and is shown below in its general form [17].

$$y_{n+1} = y_n + h\left(\frac{3}{2}f(t_n, y_n) - \frac{1}{2}f(t_{n-1}, y_{n-1})\right). \quad (66)$$

The Adams-Bashforth scheme is an explicit, two-step method which requires the solution of y_n and y_{n-1} to solve for the next value, y_{n+1} . h is the step size. To discretize the Navier-Stokes equation in time the Adams-Bashforth scheme is substituted into equation (2) to achieve the following set of iterative equations shown below. The Adams-Bashforth scheme is applied only on advection and viscous terms, but not for the pressure because it does not have a time derivative.

$$\frac{u_i^{n+1} - u_i^n}{\Delta t} = \frac{3}{2}g(u_i^n) - \frac{1}{2}g(u_i^{n-1}) - \frac{\delta P^{n+1}}{\delta x_i}. \quad (67)$$

The function $g(u_i^n)$ is the sum of the advection and viscous terms and is defined as follows.

$$g(u_i^n) = -u_j^n \frac{\delta u_i^n}{\delta x_j} + Re_\tau^{-1} \frac{\delta^2 u_i^n}{\delta x_j^2}. \quad (68)$$

$\frac{\delta}{\delta x_j}$ is representing an approximation of the spatial derivatives. The pressure is here evaluated at the next time step, as indicated by equation (67). The problem that arises is that we have two unknowns, assuming values of the n -th and $n-1$ -th are known, P^{n+1} and u^{n+1} . A working solution to this problem is to divide equation (67) into

two equations, a predictor and a corrector. By defining a temporary quantity, u_{i*} , as follows

$$u_{i*} = u_i^{n+1} + \Delta t \frac{\delta P^{n+1}}{\delta x_i} \quad (69)$$

it is easily shown, by rearranging equation (67), that

$$u_{i*} = u_i^n + \frac{3}{2} \Delta t g(u^n) - \frac{1}{2} \Delta t g(u^{n-1}). \quad (70)$$

The right hand side of the latter equation contains only known quantities. By taking the divergence of equation (69) the following is achieved.

$$\frac{\delta u_{i*}}{\delta x_i} = \frac{\delta u_i^{n+1}}{\delta x_i} + \Delta t \frac{\delta^2 P^{n+1}}{\delta x_i}. \quad (71)$$

Mass conservation still applies and from that it follows that $\frac{\delta u_i^{n+1}}{\delta x_i} = 0$. Equation (71) now becomes

$$\frac{\delta^2 P^{n+1}}{\delta x_i} = \frac{\delta u_{i*}}{\delta x_i} \frac{1}{\Delta t}. \quad (72)$$

This is a Poisson equation for the pressure. The temporary quantity u_{i*} is first solved and is then used in the Poisson equation to solve for the pressure. Then the next step velocity is found. According to Gillisen [16], p. 39, the Poisson equation is solved using a tri-diagonal matrix solver. Homogeneous directions are transformed and solved in Fourier space.

4.4.4 BOUNDARY AND INITIAL CONDITIONS

In the homogeneous directions, x and y , all variables use periodic boundary conditions which means that at the inlet and outlet the respective variables are equal at each time step. At the walls, $z = 0$ and $z = 1$, the no-slip condition is used

$$u_{z=0} = u_{z=1} = 0. \quad (73)$$

As mentioned earlier, the velocity in the wall-normal direction are computed in the cell centers. To fulfill the boundary conditions and enforce zero derivatives on the walls the following is used, respectively:

$$u(z_0^C) = -u(z_1^C), \quad u(z_{N_z}^C) = -u(z_{N_z+1}^C), \quad (74)$$

$$u(z_0^C) = u(z_1^C), \quad u(z_{N_z}^C) = u(z_{N_z+1}^C). \quad (75)$$

The initial conditions for the velocities and the pressure can be obtained by either using a random velocity field or using a fully developed turbulent velocity field from previous simulation. For the case with grid points of $48 \times 48 \times 192$, a previous simulation of a fully developed turbulent velocity field was used, but the rest of the simulations used a random velocity field.

4.5 COMPUTATIONAL MESH AND DOMAIN

The simulations performed in this thesis are divided into multiple cases. In total there are eight simulations divided into four cases. Before briefly introducing the different cases, some background information about the simulations will be presented which are applicable to all of them.

Figure (1) shows the channel flow that are used in all simulations, though with different grid resolutions and domain sizes. The height, width and length are denoted as l_z , l_y and l_x , respectively. For the simulations Fortran is used as the programming language and is parallelized using the Message Passing Interface (MPI). The parallelization is used to be able to utilize the power of multiple processors simultaneously. This is done by dividing the wall-normal direction into multiple parts. Each processor will be used to solve the Navier-Stokes equations on each corresponding part. The grid point variables in the top and bottom layers of each part is known to the adjacent parts and are used in the computations. The data in the streamwise direction is divided into parts. This is done in regards to solving the Poisson equation (72), where the data are transposed into the different parts, solved, and then the pressure data are transposed back ([16], p. 31). The supercomputer used for the simulations is called Stallo. For all simulations the number of processors used was 16, except for the last simulation, $192 \times 192 \times 192$, which used 64.

As mentioned there were in total eight different simulations divided into four cases: Coarse-grid, Short-domain, Narrow-domain and Large-domain simulations. The subsections below will briefly introduce the different cases.

4.5.1 COARSE-GRID SIMULATIONS

The first case is Coarse-grid. This is a series of three simulations with what is considered a series of low resolution simulations combined with a small domain, shown in Table (2). The two purposes of this case are to compare the simulations with data from Kim et al.[1] and also to see how different quantities are affected by coarse grid simulations. This is a small domain case compared to what was done in Kim et al.[1], so by comparing the simulations it can also show which grid resolutions are sufficient and which are not.

4.5.2 SHORT-DOMAIN SIMULATIONS

The second case consists of two simulations, with the purpose to see how the streamwise length, l_x , affect the different quantities and also compare it to Kim et al.[1] for

Grid resolution ($N_x \times N_y \times N_z$)	Domain Size (l_x, l_y, l_z)
24x24x96	1.5, 0.75, 1
48x24x96	1.5, 0.75, 1
48x48x192	1.5, 0.75, 1

Table 2: Grid resolutions and domain size for the Coarse-domain case

Grid resolution ($N_x \times N_y \times N_z$)	Domain Size (l_x, l_y, l_z)
96x48x192	3.0, 0.75, 1
192x48x192	6.0, 0.75, 1

Table 3: Grid resolutions and domain size for the Short-domain case

verification. The domain size and grid resolutions for the two simulations are shown in Table (3).

4.5.3 NARROW-DOMAIN SIMULATIONS

This case consists of two simulations where instead of the streamwise length, the spanwise width is increased. Here the purposes are to see the effect of greater width and then again to verify with Kim et al.[1]. The work done by Kim et al. works as a reference; it has been widely verified by peers and known to be reliable. Table (4) shows the grid resolutions and the domain sizes used in this case.

4.5.4 LARGE-DOMAIN SIMULATIONS

The last case consists of one simulation where both the channel length and channel width are increased four times the base domain size of $l_x = 1.5$ and $l_y = 0.75$, to $l_x = 6$

Grid resolution ($N_x \times N_y \times N_z$)	Domain Size (l_x, l_y, l_z)
48x96x192	1.5, 1.5, 1
48x192x192	1.5, 3.0, 1

Table 4: Grid resolutions and domain size for the Narrow-domain case

Grid resolution ($N_x \times N_y \times N_z$)	Domain Size (l_x, l_y, l_z)
192x192x192	6.0, 3.0, 1

Table 5: Grid resolutions and domain size for the Large-domain case

and $l_y = 3$ as shown in Table (5). The purposes of this case are to see how much better the obtained results are compared to the two latter cases and then be able to conclude which of the directions that have the greatest effect on the turbulence statistics.

Part II

RESULTS

RESULTS

The results presented in this thesis are divided into four main cases: Coarse-grid, Short-domain, Narrow-domain and Large-domain, with different grid resolutions and domain sizes. The purpose is to see how different grid resolutions and domain sizes affect the turbulent quantities, and they are then compared with experiments done by Kim et al.[1] for verification purposes. The results will be presented illustratively using graphs along with brief comments. The results are processed from a statistically steady state velocity field with $Re_\tau = 360$. Kim et al.[1] are using a Reynolds number of 180, but this is essentially the same because they are using only half the channel, which is sufficient due to symmetry. For the comparisons only half the channel is used. The structure of how the results are presented, for all cases, is more or less the same as in Kim et al.[1].

5.1 COARSE GRID SIMULATIONS

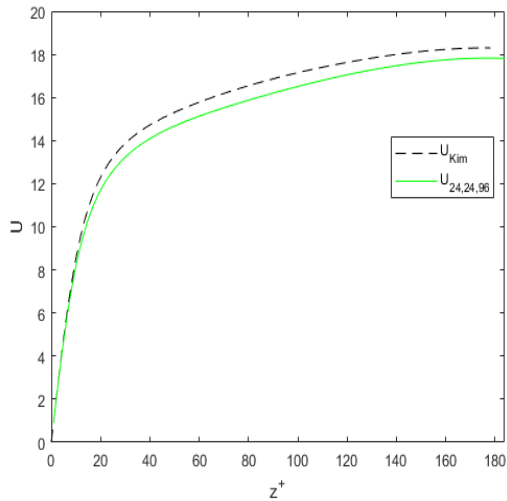
The Coarse grid simulations consists of three simulations as shown in Table (2). The initial conditions are set using a random velocity field for the first two simulations and for the last simulation, $48 \times 48 \times 192$, a fully developed turbulent velocity field from a previous simulation is used. The simulations performed in this case have very coarse grid resolutions and small domain sizes. DNS is usually used in much higher grid resolutions and bigger domain sizes, in which have been done in the other cases shown in the next two sections. With that in mind, the results obtained in this case are very good.

5.1.1 MEAN PROPERTIES

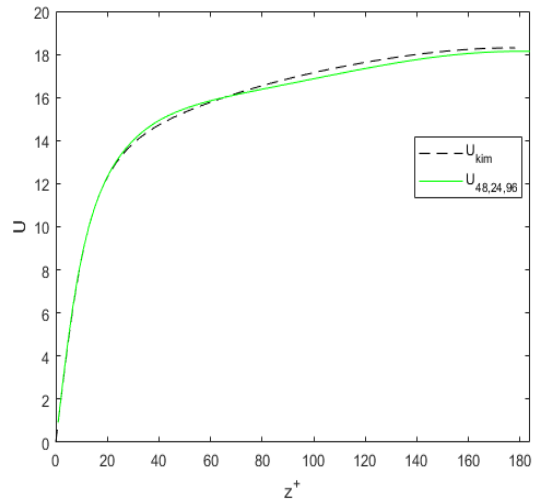
The normalized mean velocity profiles of simulations with increasing grid resolutions, compared with data from Kim et al.[1], can be shown in Figure (4). Close to the wall they correspond very well, but going further out towards the center of the chan-

nel the discrepancies starts to increase. The velocities of the performed simulations are slightly below the mean bulk velocity from Kim's simulation. With increasing grid resolutions, the results correspond better with the results of Kim et al. The mean bulk velocity is defined by

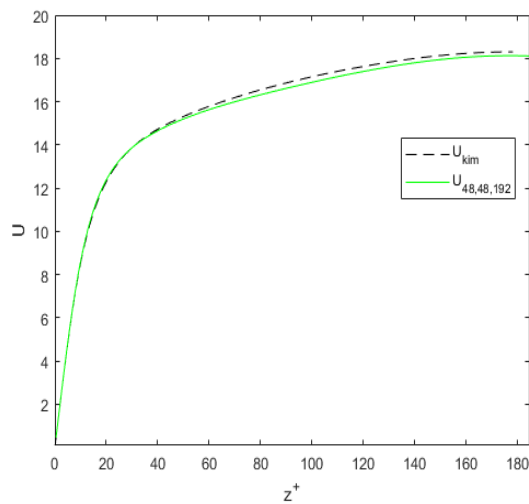
$$U_m \equiv \frac{1}{l_z} \int_0^{l_z} U dz. \quad (76)$$



(a) Grid resolution of 24x24x96



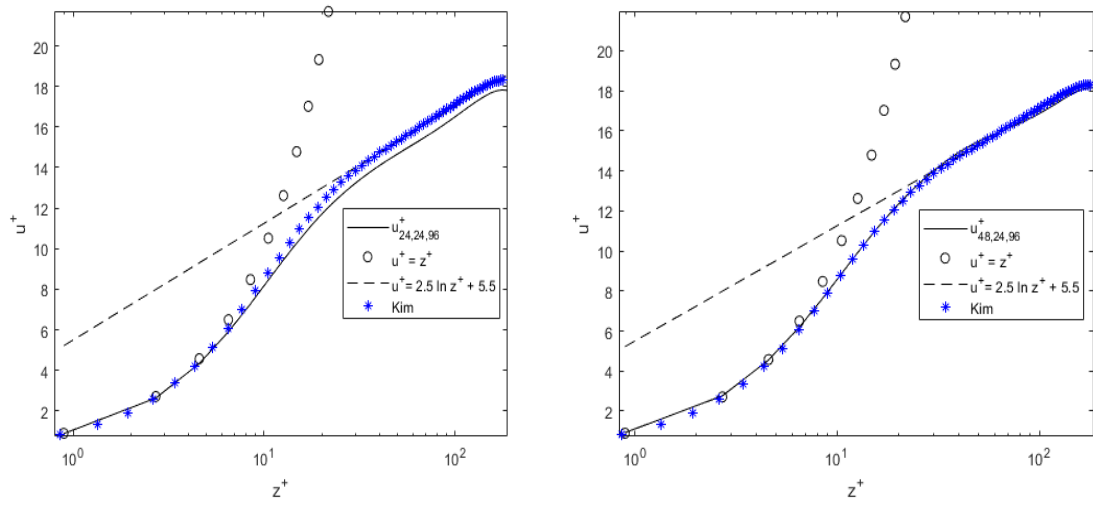
(b) Grid resolution of 48x24x96



(c) Grid resolution of 48x48x192

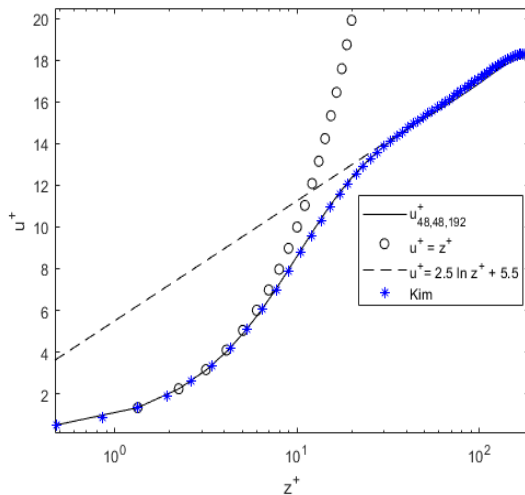
Figure 4: Normalized mean velocity profile for different simulations compared with data from Kim et al.[1]

To see how the velocity profile corresponds to the law of the wall, described in Chapter (3.2), a logarithmic plot of the three simulations against the equations of the law of the wall is created and shown in Figure (5). The velocity profiles are in agreement with the law of the wall and it is easily seen that the higher the grid resolution, the better the velocity profile will follow the law. The mean velocity is caused by large scale motion and should not be much affected by the grid resolution. This will be discussed more in the next chapter.



(a) Grid resolution of 24x24x96

(b) Grid resolution of 48x24x96



(c) Grid resolution of 48x48x192

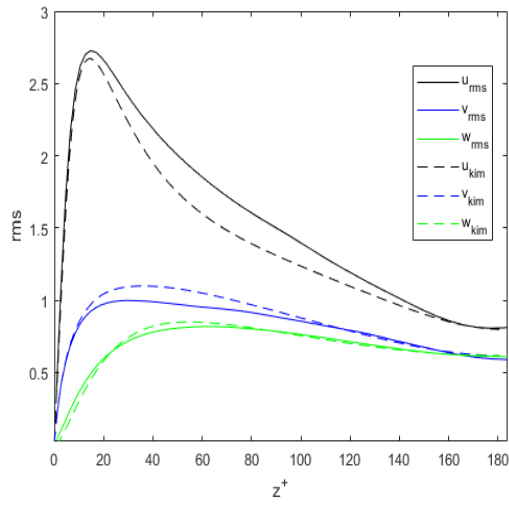
Figure 5: Velocity profile close to the wall, in logarithmic scale, compared with data from [1]

5.1.2 TURBULENCE INTENSITIES

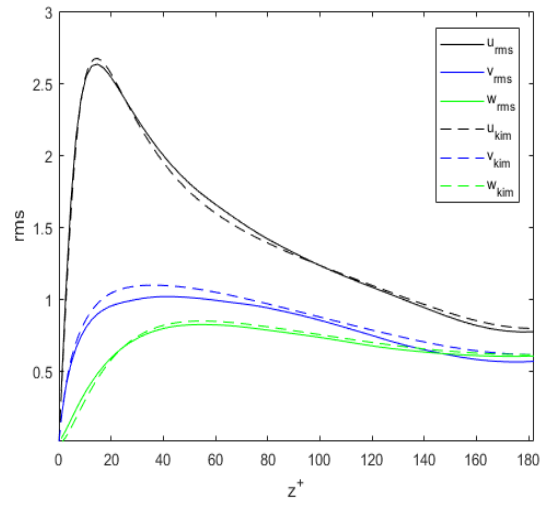
Turbulence intensity can be characterized as a measure of turbulence, often as a percentage. Here, the root mean square (rms) value of the velocity fluctuations are used as the turbulence intensity. Figure (6) shows the rms values of the velocity fluctuations for the different simulations in all three directions for the half channel. The velocity fluctuations, also called the turbulent fluctuations, are caused by large scale eddies and should not be much affected by different grid resolutions. The rms value of the velocity fluctuations are calculated using the following equation.

$$u_{rms,i} = \sqrt{u_i^2}. \quad (77)$$

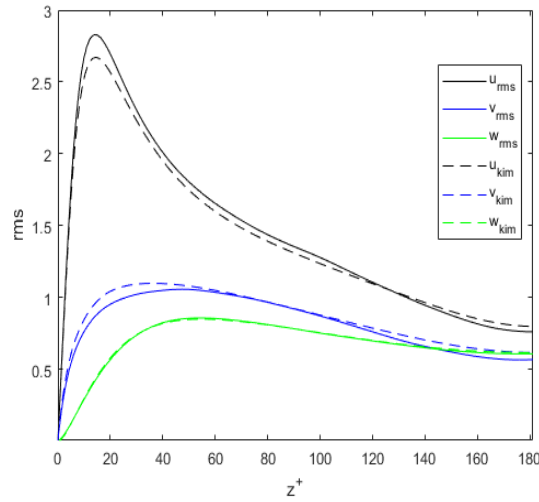
In Figure (6) we still see some discrepancies, especially between the $24 \times 24 \times 96$ simulation and the other two simulations around $20 < z^+ < 130$. For the maximum value of u_{rms} , around $z^+ = 20$, we see that u_{rms} for $24 \times 24 \times 96$ slightly overestimates, $48 \times 24 \times 96$ slightly underestimates and $48 \times 48 \times 192$ is overestimating more. At $z^+ > 20$ the discrepancies for $48 \times 24 \times 96$ and $48 \times 48 \times 192$ are smaller than for $24 \times 24 \times 96$. It is difficult to see a clear trend in increasing grid resolution. Other than that it seems that increasing the grid resolution will give results that correspond better with Kim's results.



(a) Grid resolution of 24x24x96



(b) Grid resolution of 48x24x96



(c) Grid resolution of 48x48x192

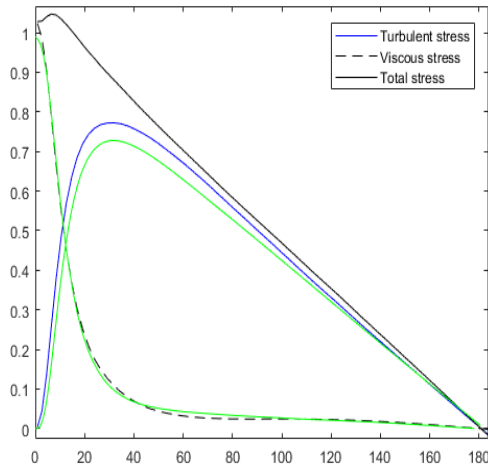
Figure 6: The rms values of the velocity fluctuations for different simulations compared with data from [1]

5.1.3 REYNOLDS SHEAR STRESS

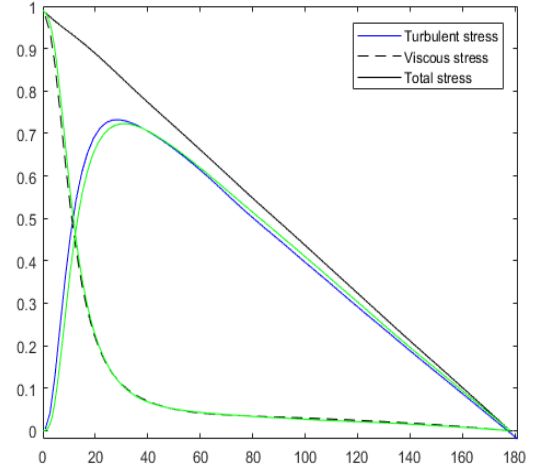
The Reynolds stress is a matrix consisting of nine components, as shown in the equation below, and accounts for turbulent motion as discussed in Chapter (2.3). The Reynolds stress matrix is given by the following matrix.

$$\overline{u_i u_j} = \begin{bmatrix} \overline{uu} & \overline{uv} & \overline{uw} \\ \overline{vu} & \overline{vv} & \overline{vw} \\ \overline{wu} & \overline{wv} & \overline{ww} \end{bmatrix} \quad (78)$$

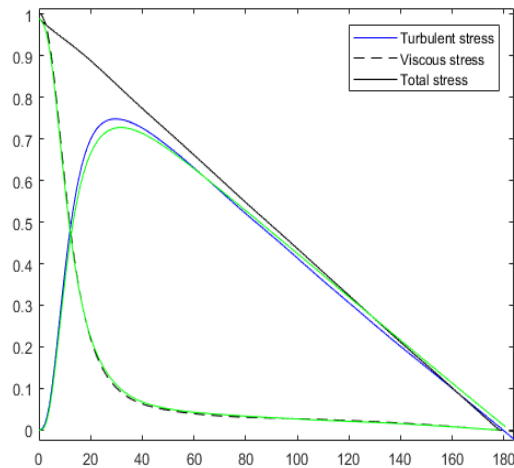
Due to the symmetric property of the tensor it represents only six unknowns. The diagonal components are called Reynolds normal stresses and they are the squared values of the rms values of the velocity fluctuations, which will not give more information than what was given in the previous subsection. They will therefore not be considered further. The other components in the tensor are called Reynolds shear stresses. The components \overline{uv} , \overline{vw} and their corresponding symmetrical components are very close to zero, and will not be considered further. The important component is \overline{uw} , and will be analyzed further in this section. Equation (37) physically means that the total shear stress consists of two terms; the viscous shear stress and the Reynolds shear stress. Figure (7) shows the viscous shear stress and the Reynolds shear stress compared to Kim's results, shown in green straight lines. It also shows the total shear stress, shown in straight black line. The total shear stress should in theory be a straight line, and the only grid resolution to notably deviate from a straight line is the 24x24x96 simulation. For grid resolutions the viscous stress fits well with Kim's data, while the turbulent shear stress have some discrepancies, especially between $z^+ = 20$ and $z^+ = 40$, but gradually improving with finer grid resolutions.



(a) Grid resolution of 24x24x96



(b) Grid resolution of 48x24x96



(c) Grid resolution of 48x48x192

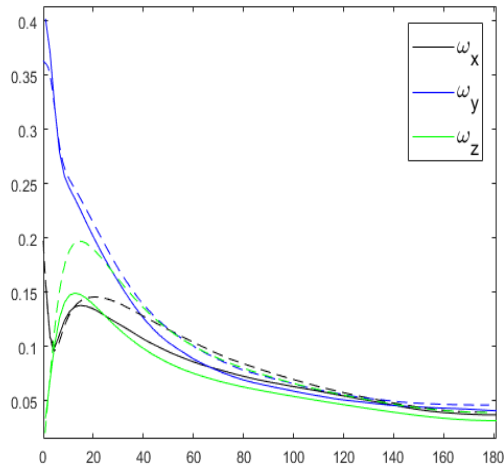
Figure 7: The viscous, turbulent and total shear stress for increasing grid resolutions compared with data from [1]

5.1.4 VORTICITY

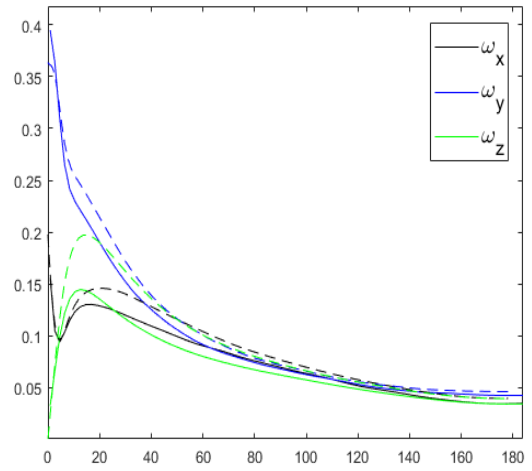
In turbulence the large rotating eddies are broken down into smaller rotating eddies, as discussed in Chapter (2.2.4). This means that during the whole existence of turbulence, vorticity exists. It is therefore interesting to look at how the vorticity change over the course of the channel. Vorticity, $\vec{\omega}$, is a vector that measures the rotation at the points in the flow and is defined by the following equation.

$$\vec{\omega} = \nabla x \vec{V}. \quad (79)$$

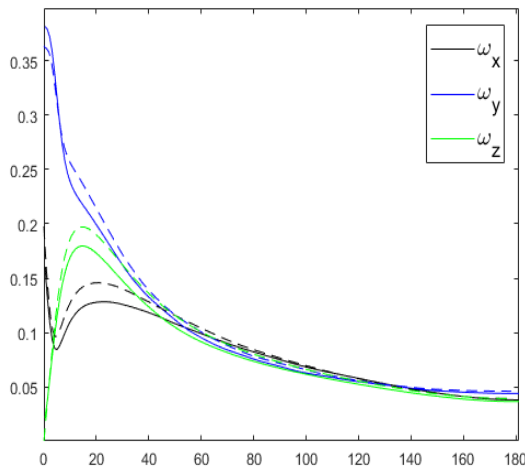
This equation mathematically means that the vorticity is the curl of the velocity field. Calculation of the rms value of the vorticity fluctuations is done by using the mathematical expression, $\omega_i v / u_\tau^2$. Figure (8) shows the different components of the rms value of the vorticity fluctuations for the different simulations. Kim's data are shown in dashed lines. From the figure it can be shown that the wall-normal component is significantly better in $48x48x192$ than in the other two. The other components do gradually improve. Close to the wall the different components seem to be dependent of direction, also called anisotropic, but further out they become isotropic, which means they are independent of direction. Vorticity is mainly caused by small scale motion and should be affected by change in grid resolution. There are noticeable discrepancies compared to Kim's data in all directions and throughout the height of the channel.



(a) Grid resolution of 24x24x96



(b) Grid resolution of 48x24x96



(c) Grid resolution of 48x48x192

Figure 8: The rms value of the vorticity fluctuations for increasing grid resolutions compared with data from [1]

5.1.5 DISSIPATION

The dissipation components ϵ_{11} , ϵ_{22} and ϵ_{33} for the different cases compared to results from Kim et al.[1] are shown in Figure (9). The components are computed using equation (28). For ϵ_{11} the simulated cases all have a discrepancy close to the wall compared to Kim's data, but moving further away from the wall the discrepancy gets smaller and at around $z^+ = 80$ they seem to coincide. This behaviour is expected, and applies to all components, because the dissipation is getting smaller

further away from the wall and thus there are less discrepancies. For ϵ_{22} it seems that the coarser the grid resolution, the better results will be obtained. The dissipation is mainly caused by small eddies and should normally be affected by the grid resolution not the domain sizes. This behaviour will be discussed more in the next chapter. For ϵ_{33} the data fits well with the theory that dissipation is affected by the grid resolution and improves significantly with finer grid resolution.

Figure (10) shows the total dissipation, ϵ , again compared with Kim's results. ϵ is computed using the last term in equation (27). From the figure it is shown that it has more or less the same shape as ϵ_{11} . This is expected because ϵ_{11} is bigger than the other two components and therefore contributes more. The discrepancy is small for all simulations compared to each other but significant compared to Kim's data.

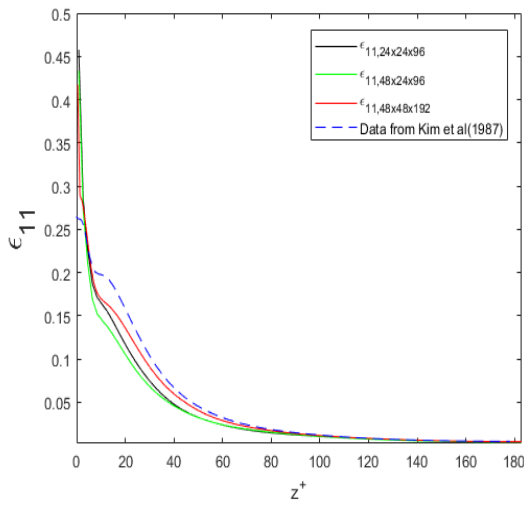
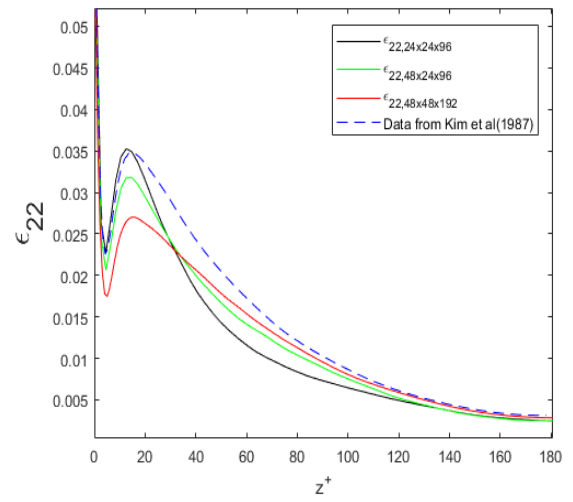
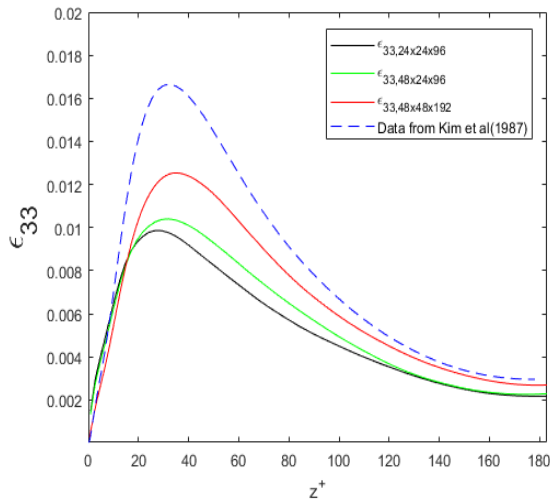
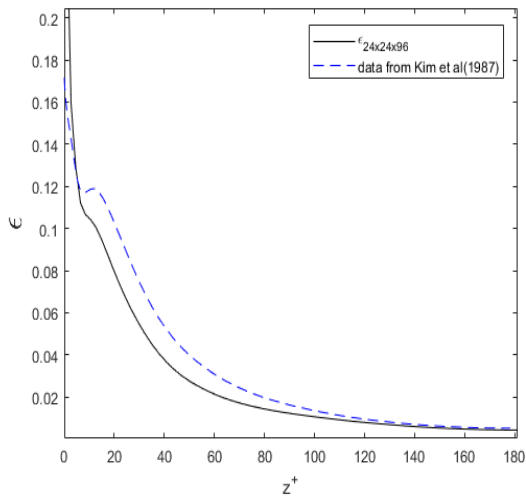
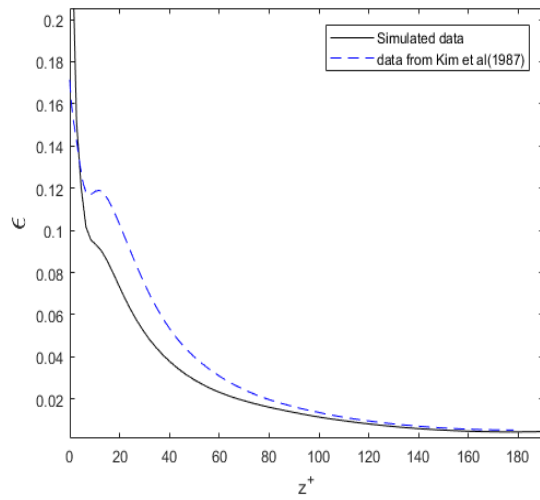
(a) ϵ_{11} for increasing grid resolutions.(b) ϵ_{22} for increasing grid resolutions.(c) ϵ_{33} for increasing grid resolutions.

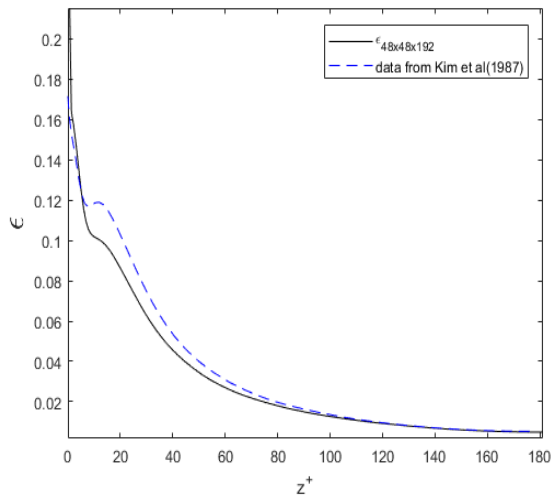
Figure 9: The dissipation components for increasing grid resolutions compared with data from [1]



(a) Grid resolution of 24x24x96



(b) Grid resolution of 48x24x96



(c) Grid resolution of 48x48x192

Figure 10: The total dissipation for increasing grid resolutions compared with data from [1]

.

5.2 SHORT DOMAIN SIMULATIONS

The aim of this case is to see how the length, l_x , in the streamwise direction is affecting the turbulent quantities. The streamwise length is doubled two times and should give noticeable results because the base domain size, $l_x = 1.5$ and $l_y = 0.75$, is a short domain. The grid resolution in the streamwise direction is also changed so as to keep $\Delta x = l_x/N_x$ constant. This will make sure the resolution is unchanged, and

therefore should theoretically only be a domain size effect. It consists of two simulations, as shown in Table (3), where they are compared to each other and to the results from Kim et al. The finest grid resolution from the Coarse-grid case, $48 \times 48 \times 192$, is included here for comparison. The two simulations used a random velocity profile to obtain the initial conditions.

5.2.1 MEAN PROPERTIES

The mean velocity profiles are shown in Figure (11). It seems that increasing channel length gives greater mean velocity. The discrepancy between them is very small. The mean velocity is mainly caused by large scale motion and should therefore be more affected by the domain size than the grid resolution.

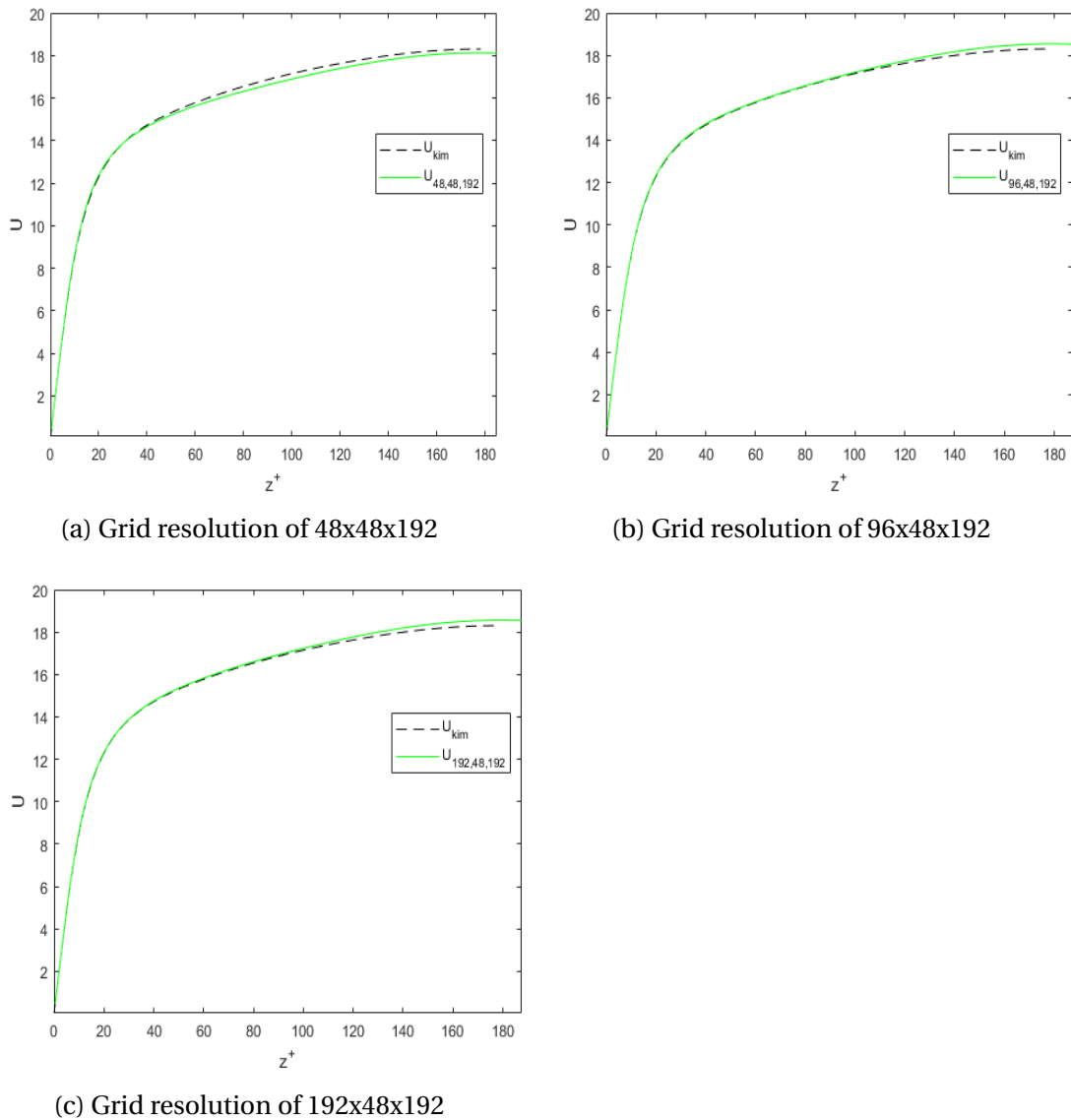
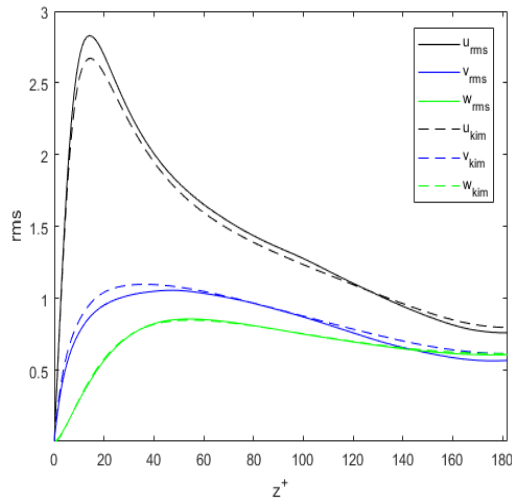


Figure 11: The mean velocity profile for the Short-domain case for increasing streamwise domain size, l_x , compared with data from Kim et al.[1]

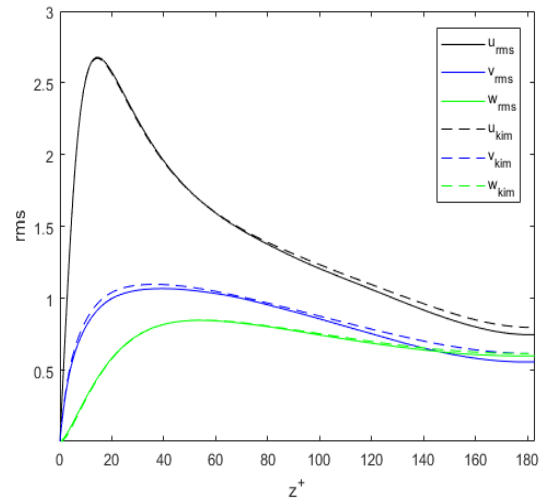
5.2.2 TURBULENCE INTENSITIES

Figure (12) shows the rms values for increasing the streamwise length of the domain. The u_{rms} is over predicted in the 48x48x192 simulation at around $z^+ = 15$ and then going towards the half channel it under predicts. For the 96x48x192 simulation it is very close to Kim's data until around $z^+ = 70$ and then under predicts all the way to the half channel. The v_{rms} seems to under predict over almost the whole range of the half channel. The last simulation is very close to Kim et al.[1]. Increasing the

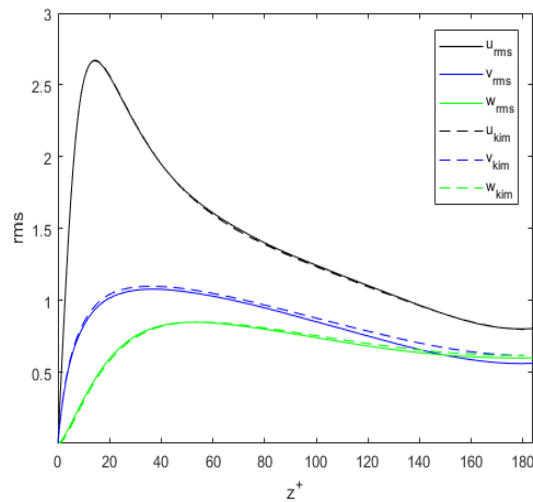
streamwise domain size gives better results for both u_{rms} and v_{rms} while for w_{rms} they do not change much between the simulations and discrepancies between them are very small.



(a) Grid resolution of 48x48x192



(b) Grid resolution of 96x48x192

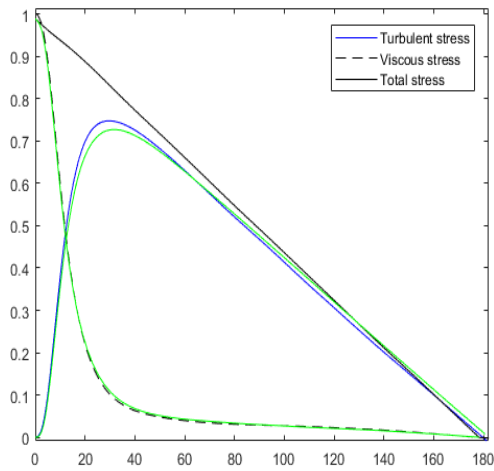


(c) Grid resolution of 192x48x192

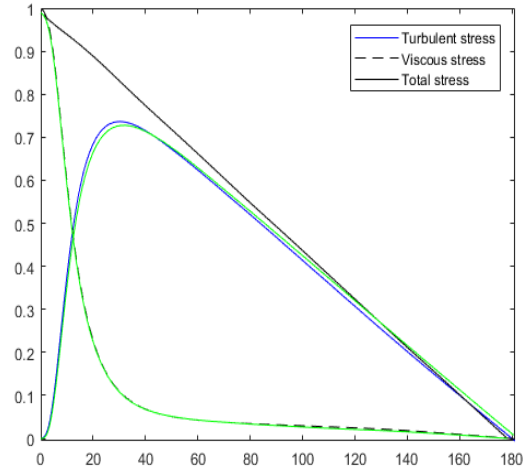
Figure 12: The rms value of the velocity fluctuations for the Short-domain case for increasing streamwise domain size, l_x , compared with data from Kim et al.[1]

5.2.3 REYNOLDS SHEAR STRESS

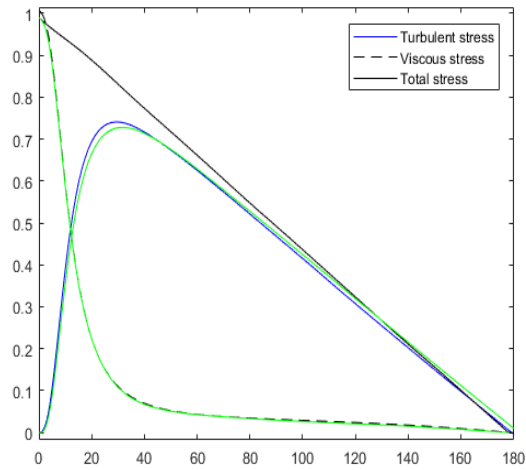
Figure (13) shows the Reynolds, viscous and total shear stress. Again, the viscous stress is also here corresponding well with Kim's data almost without noticeable discrepancies. The turbulent stress gives slightly better results by increasing the channel length.



(a) Grid resolution of 48x48x192



(b) Grid resolution of 96x48x192

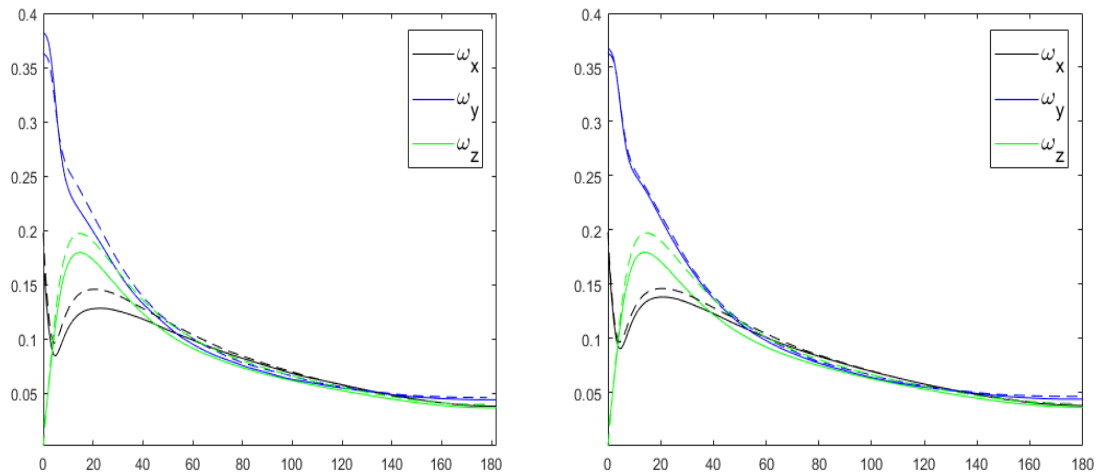


(c) Grid resolution of 192x48x192

Figure 13: The Reynolds shear stress, viscous shear stress and total shear stress for the Short-domain case for increasing streamwise domain size compared with data from Kim et al.[1]

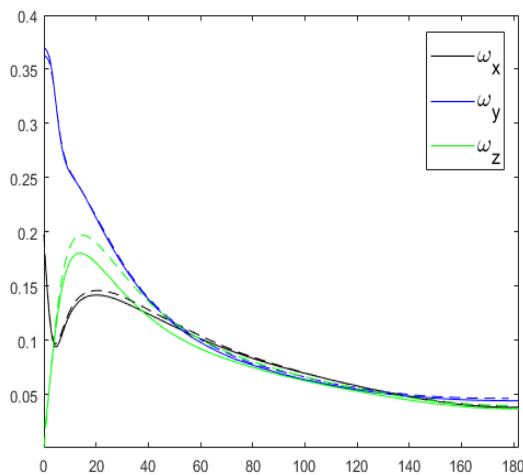
5.2.4 VORTICITY

Figure (14) shows the rms value of the vorticity fluctuations. Close to the wall the x- and y-components are improving with increasing streamwise domain size, especially between $48x48x192$ and $96x48x192$, while the z-component does not give any noticeable changes. The discrepancy between $96x48x192$ and $192x48x192$ is noticeable, although very small, only in the streamwise direction. Away from the wall none of the components give any noticeable discrepancies and more or less behaves isotropically.



(a) Grid resolution of $48x48x192$

(b) Grid resolution of $96x48x192$



(c) Grid resolution of $192x48x192$

Figure 14: The rms value of the vorticity fluctuations for the Short-domain case for increasing streamwise domain size compared with data from [1]

5.2.5 DISSIPATION

Figure (15) shows the dissipation components and the total dissipation for increasing channel length. The dissipation is caused by small scale eddies and it is not expected for the dissipation to change significantly when increasing the domain size. From the figure it is clear that increasing the channel length improves the results compared to Kim's data. A secondary effect seems to occur and will be discussed further in the next chapter.

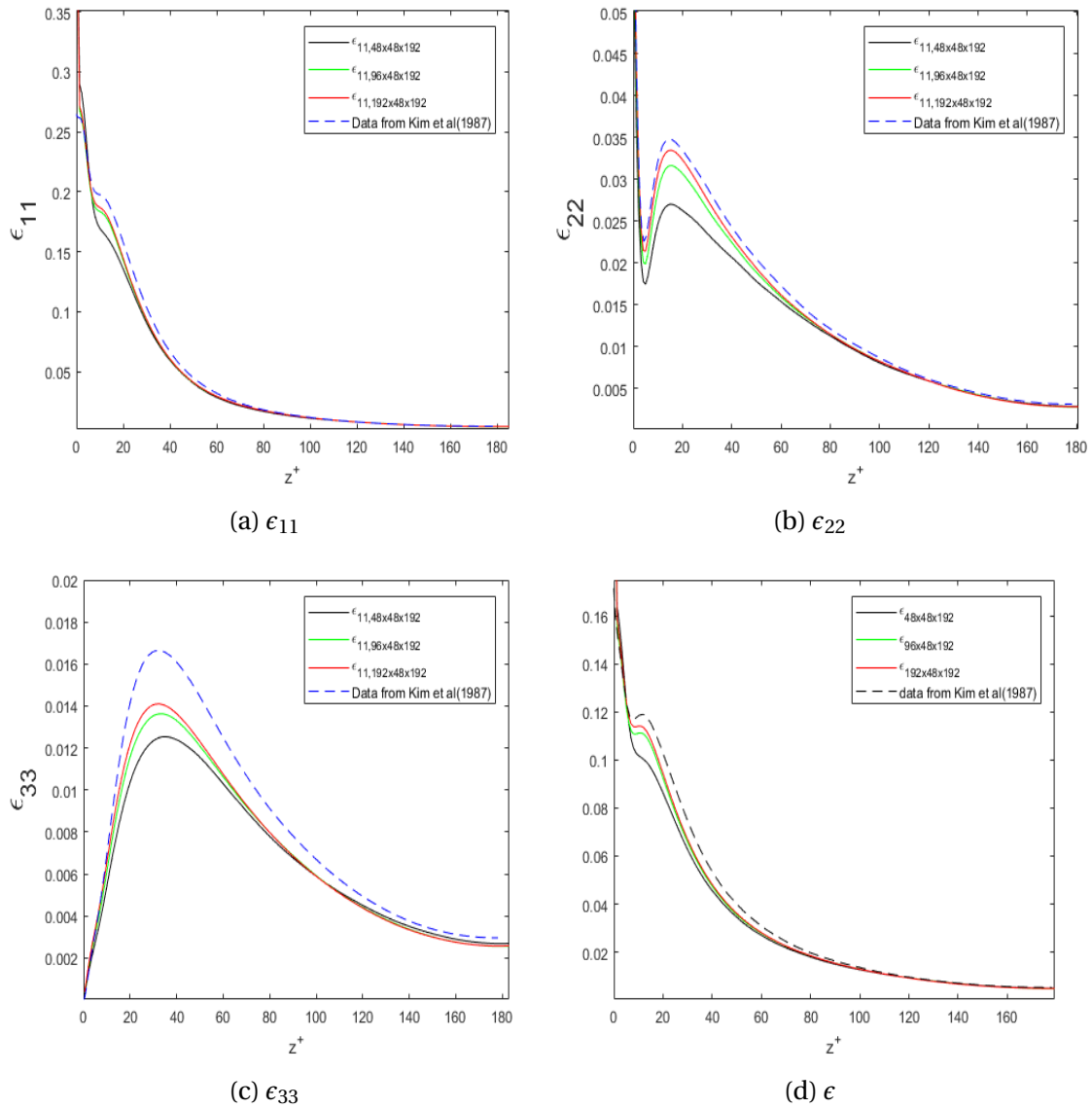


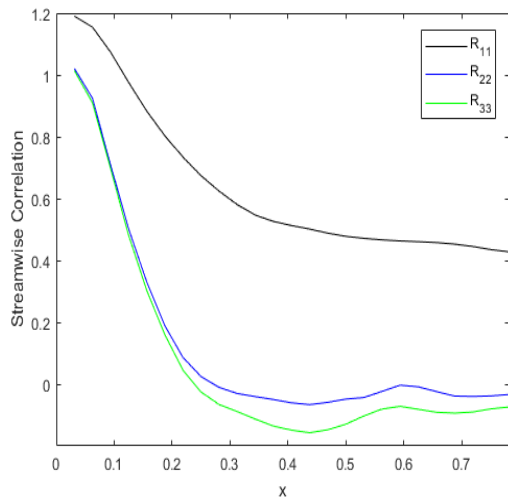
Figure 15: The dissipation components and total dissipation for the Short-domain case for increasing streamwise domain size compared with data from Kim et al.

5.2.6 TWO-POINT CORRELATION

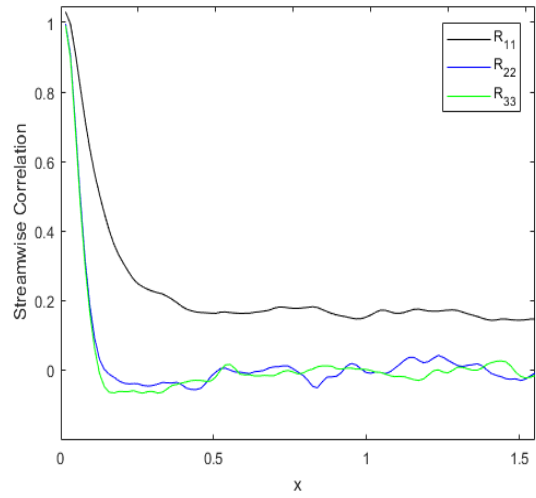
The two-point correlation is used as a tool to decide if the domain sizes are adequate. The turbulent fluctuations should be uncorrelated in the homogeneous directions. The two-point correlation is calculated using the following equation.

$$R_{ij}(\mathbf{r}, t) = \overline{u_i(\mathbf{x} + \mathbf{r}, t) u_j(\mathbf{x}, t)} \quad (80)$$

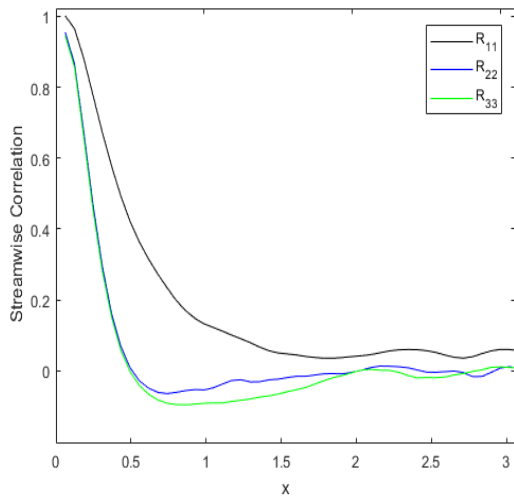
Figures (16) and (17) shows the two-point correlation, in streamwise and spanwise directions respectively, for increasing lengths of the channel at the center of the channel. The figure only shows half the channel due to symmetry. Both the streamwise and spanwise correlations are getting better and more uncorrelated for longer channels, but especially R_{11} still has a value significantly greater than zero for the streamwise correlation. For the spanwise direction it improves greatly, but deviates significantly from zero in especially R_{11} and R_{33} . It is difficult to tell whether the channel width is adequate from the two-point correlation because it is too narrow and therefore can interfere with the results.



(a) Two-point correlation for $48 \times 48 \times 192$.

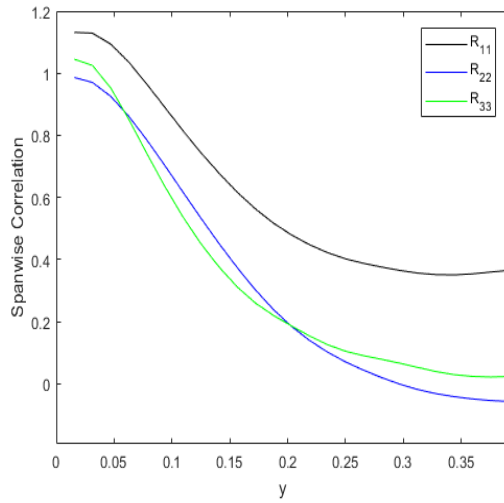


(b) Two-point correlation for $96 \times 48 \times 192$.

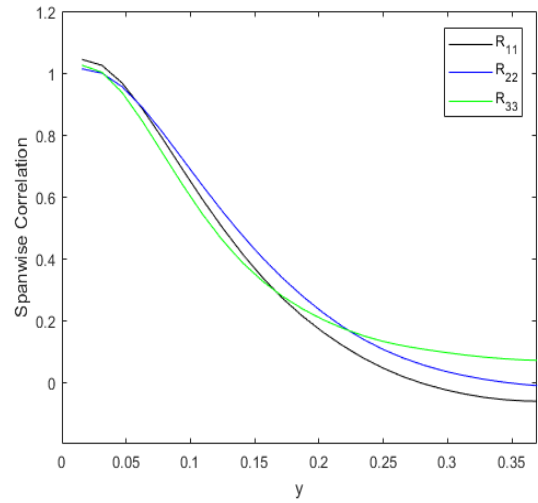


(c) Two-point correlation for $192 \times 48 \times 192$.

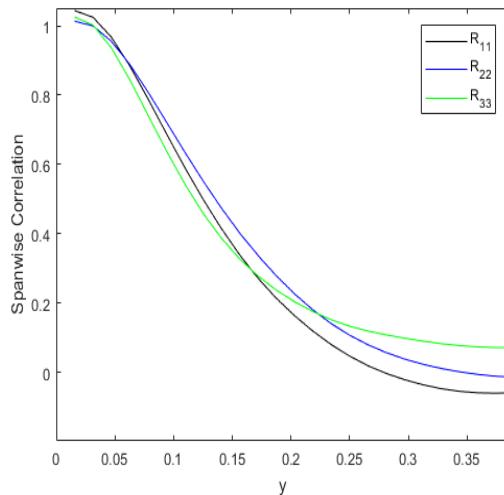
Figure 16: Two-point correlation in the streamwise direction for increased values of l_x at the center of the channel.



(a) Two-point correlation for 48x48x192.



(b) Two-point correlation for 96x48x192.



(c) Two-point correlation for 192x48x192.

Figure 17: Two-point correlation in the spanwise direction for increased values of l_x at the center of the channel.

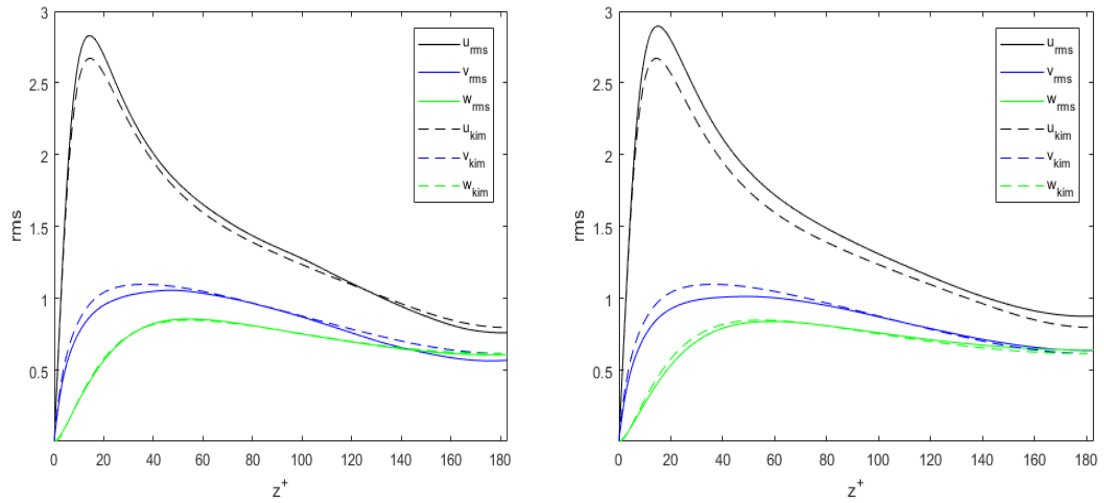
5.3 NARROW DOMAIN SIMULATIONS

In this case the domain size in the spanwise direction will be doubled in size two times from the base domain size. Here the aim is to see how an increase in channel width will affect the different turbulent quantities. This case consists of two simulations, as shown in Table (4). To conserve space the mean velocity profile is not included. The reason for not including it is that it does not have noticeable discrepancies compared to the 48x48x192 simulation which is shown in the two previous

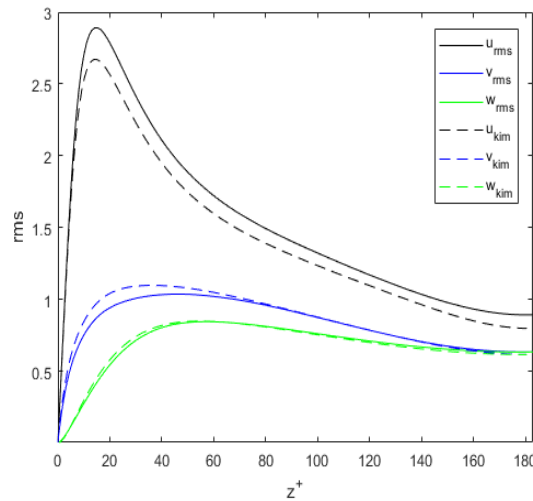
sections. The mean velocities have reached satisfying results in almost all simulations and there is not much to gain increasing the channel width nor the channel length. Again, the $48 \times 48 \times 192$ simulation is included here for comparison. To obtain the initial conditions the two simulations used a random velocity profile.

5.3.1 TURBULENCE INTENSITIES

Figure (18) shows the rms values of the velocity fluctuations and shows noticeable changes for the different simulations in the streamwise direction, while the other two directions have very small discrepancies. The discrepancies towards the results of Kim et al.[1] are significant.



(a) Rms values of velocity fluctuations for 48x48x192. (b) Rms values of velocity fluctuations for 48x96x192.



(c) Rms values of velocity fluctuations for 48x192x192.

Figure 18: Turbulence intensities for increasing channel width l_y .

5.3.2 REYNOLDS SHEAR STRESS

Figure (19) shows the viscous, turbulent and total shear stress for increasing values of the channel width. At the top of the turbulent shear stress curve there are some differences between the simulations, but other than that they are close to each other and correspond well with Kim et al.[1]. The discrepancies gradually improve with increased channel width.

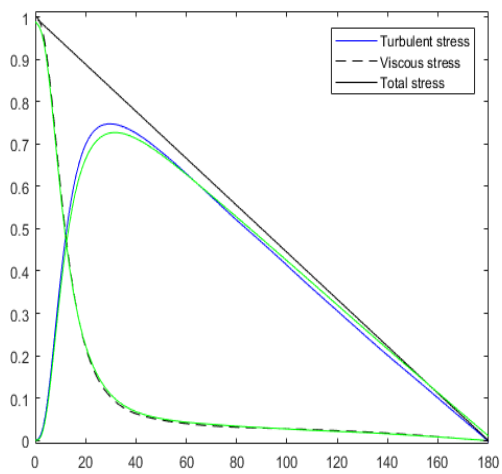
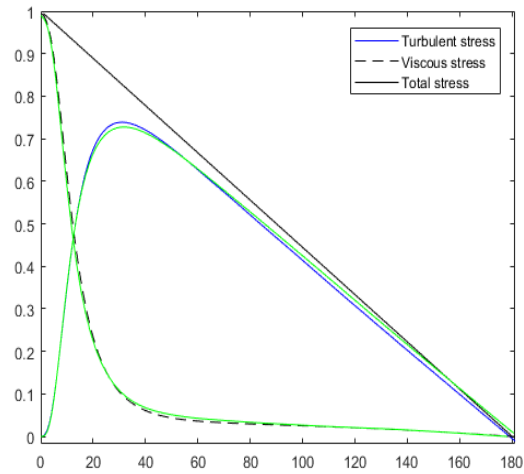
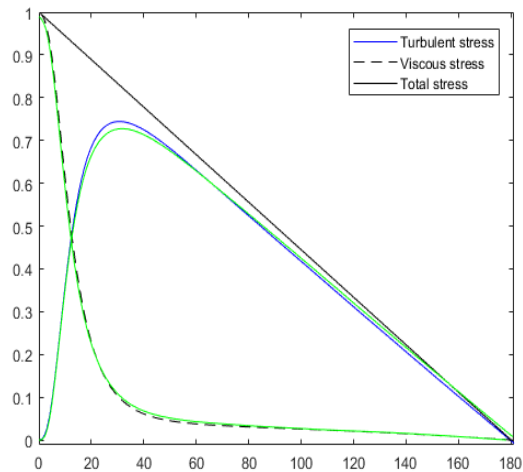
(a) Grid resolution of $48 \times 48 \times 192$.(b) Grid resolution of $48 \times 96 \times 192$.(c) Grid resolution of $48 \times 192 \times 192$.

Figure 19: Viscous, turbulent and total shear stress for increasing values of domain width l_y .

5.3.3 VORTICITY

Figure (20) shows the rms values of the vorticity, which are small scale motion and should not be much affect by domain changes. As can be seen from the figure this is also the case. None of the components change much between the simulations and correspond well with Kim's results.

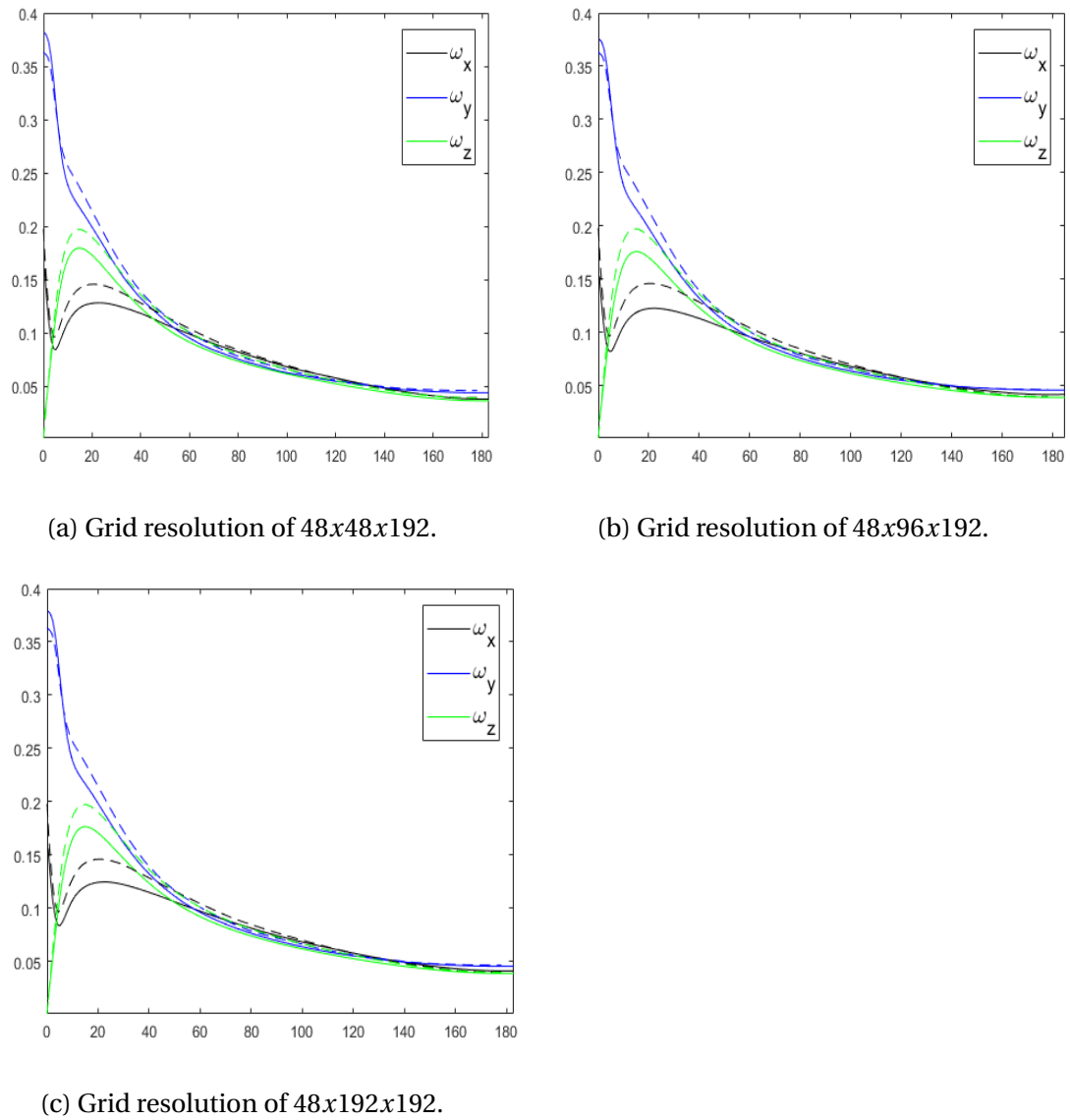


Figure 20: Rms of vorticity for increasing values of domain width l_y .

5.3.4 DISSIPATION

Figure (21) shows the dissipation components and the total dissipation for increased values of the channel width. As shown in the figure increasing the channel width does not give significantly better results and the discrepancy is small. This case shows significantly worse results compared to increasing the channel length, which gave data that changed and improved a lot between the simulations. This shows that the secondary domain effect that occurred in the Short-domain case is smaller or non-existent here.

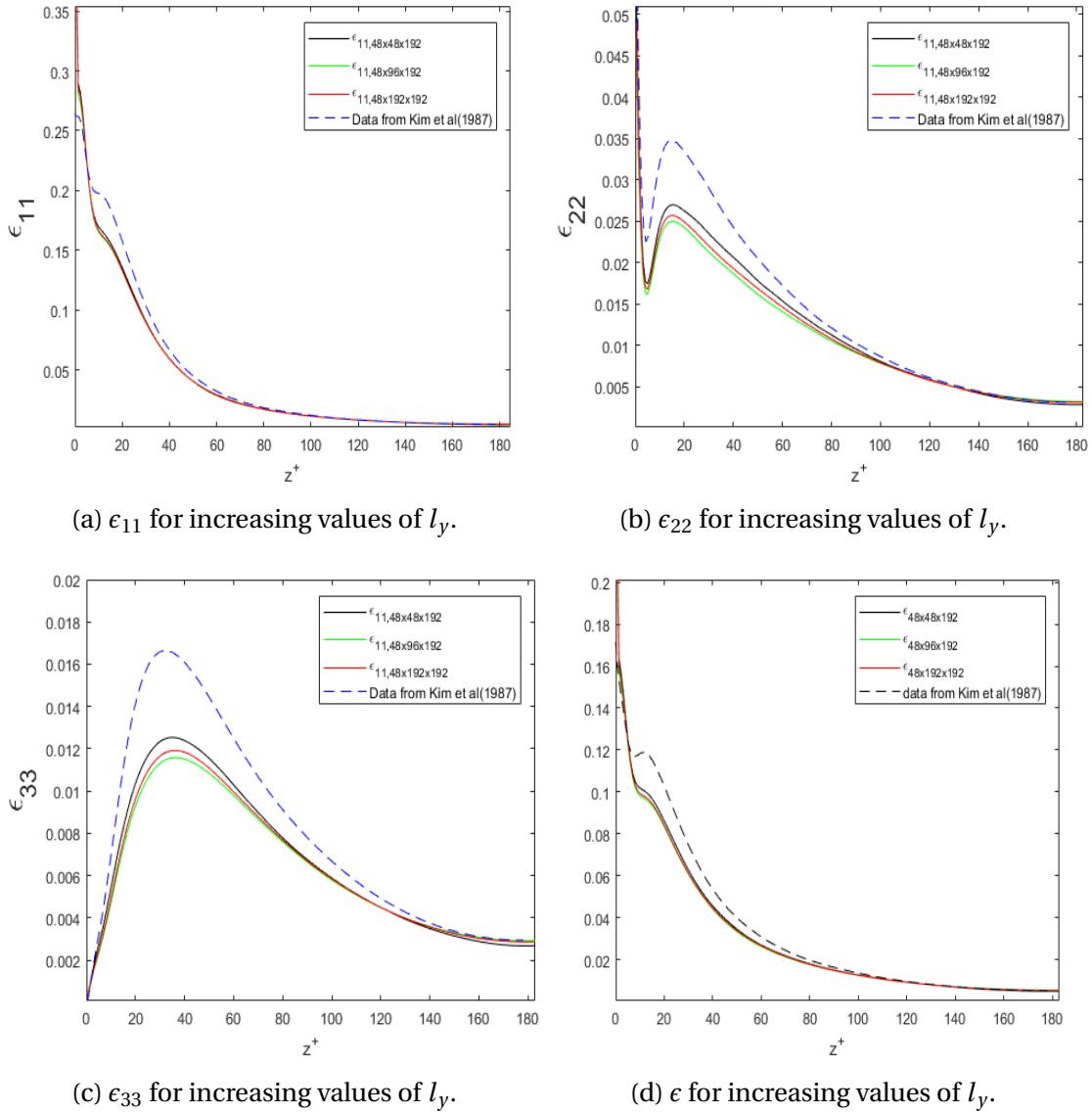
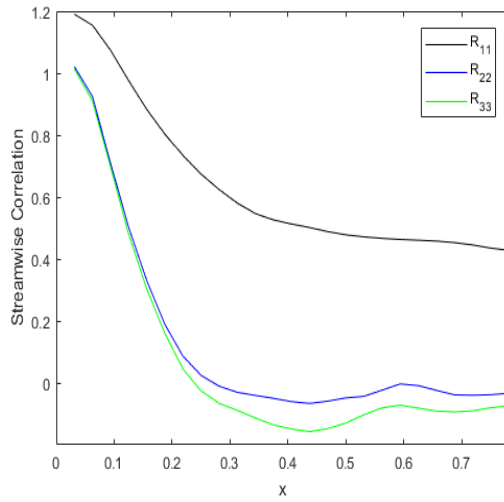


Figure 21: The dissipation components and the total dissipation for the Narrow-domain case for increasing values of the width compared with data from Kim et al.

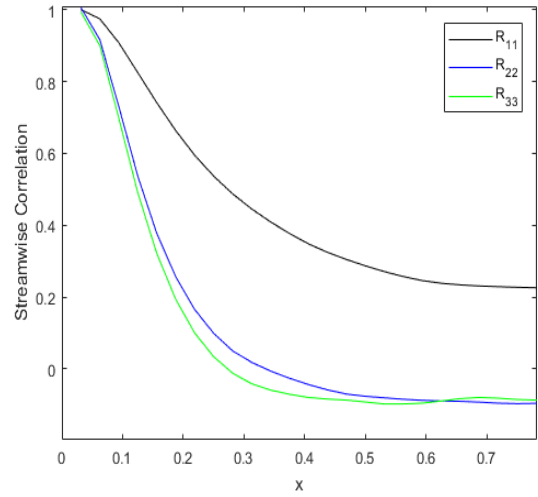
5.3.5 TWO-POINT CORRELATION

The two-point correlation in the streamwise and spanwise direction, at the center of the channel, are shown in Figures (22) and (23) respectively. In the streamwise direction the two-point correlation does not change much, but deviates much from zero and means that the channel length, $l_x = 1.5$, is too short. In spanwise direction the

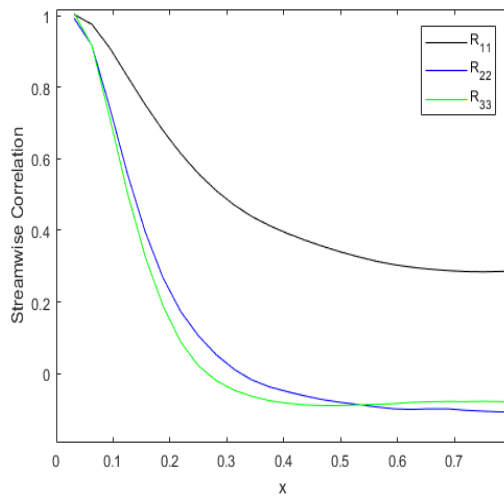
two-point correlation gradually gets better and all of the components are approaching zero, which means that the channel width is sufficiently large at $l_y = 3$.



(a) Two-point correlation for $48 \times 48 \times 192$.



(b) Two-point correlation for $48 \times 96 \times 192$.



(c) Two-point correlation for $48 \times 192 \times 192$.

Figure 22: Two-point correlation in the streamwise direction for increased values of l_x at the center of the channel.

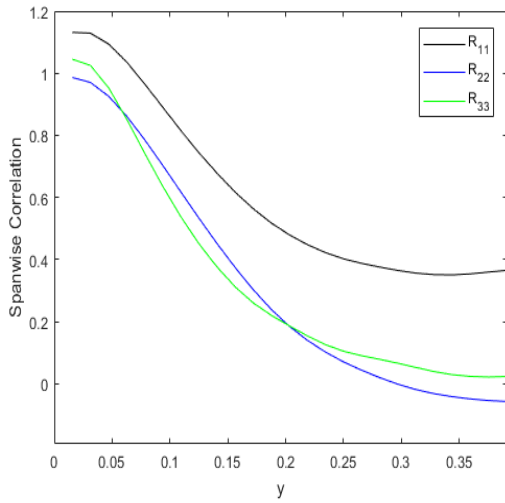
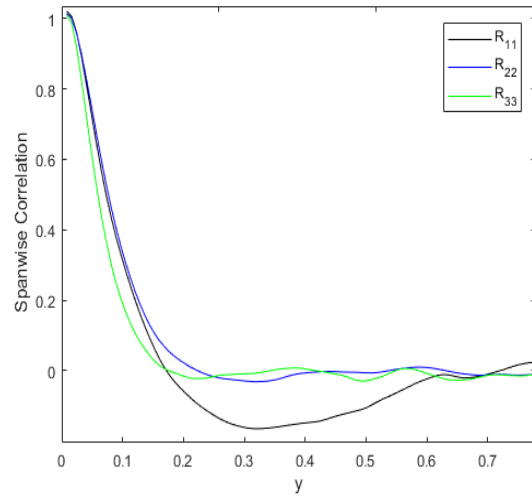
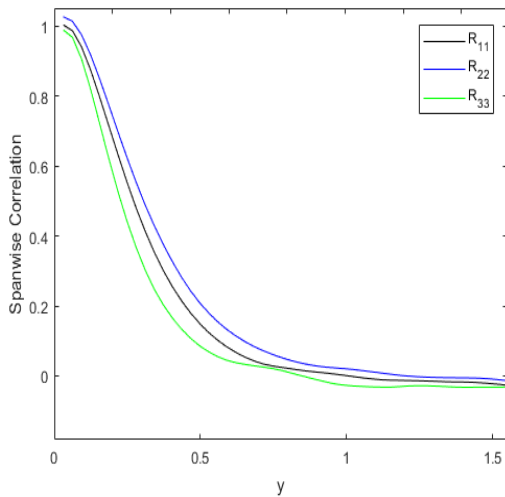
(a) Two-point correlation for $48 \times 48 \times 192$.(b) Two-point correlation for $48 \times 96 \times 192$.(c) Two-point correlation for $48 \times 192 \times 192$.

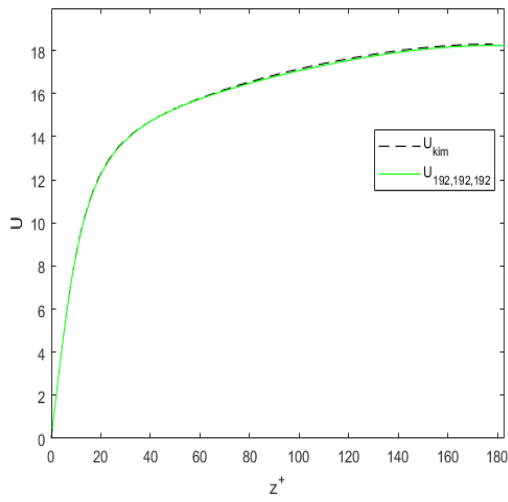
Figure 23: Two-point correlation in the spanwise direction for increased values of l_x at the center of the channel.

5.4 LARGE-DOMAIN SIMULATIONS

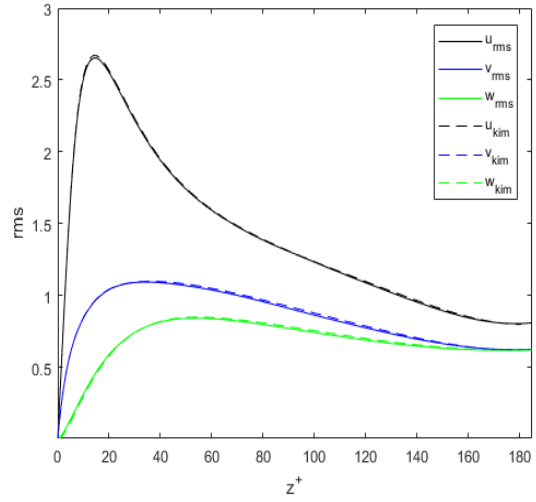
Large-domain simulations is the last case presented here and consists of one simulation with increased channel length and channel width to a domain size of $l_x = 6$ and $l_y = 3$ and grid resolution of $192 \times 192 \times 192$. From the previous two sections it is clear that the Short-domain case gives significantly better results than the Narrow-domain case, and to better be able to see the effect of a larger domain it was decided to include the Large-domain case. It is interesting to look at the different quantities

to see if the results are getting better by increasing the domain sizes in both directions. That way it can be shown which of the two directions will give better results by increasing the domain size and also show if the domain size is adequate through the two-point correlation. This domain size is nearly the same as used by Kim et al.[1], which is $4\pi\delta x 2\pi\delta x 2\delta$. This is true because Kim et al. has 2δ in wall normal direction and dividing the domain size by two will yield $2\pi\delta x \pi\delta x \delta$.

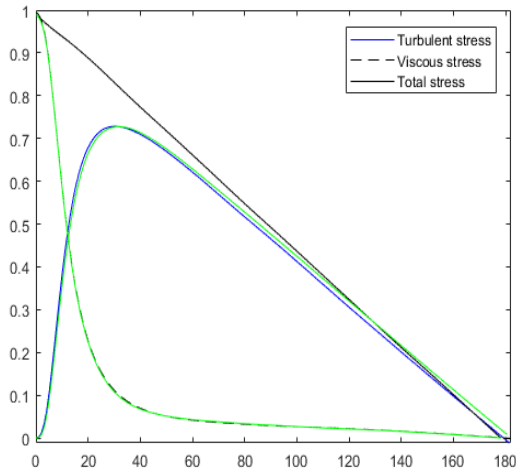
Figure (24) shows the mean velocity profile, rms value of the velocity fluctuations, viscous shear stress, turbulent shear stress, total shear stress and rms value of the vorticity. By comparing these quantities with the other previous cases it is clear that there are improvements for most of them, but there is more improvement compared to the Narrow-domain simulation than compared with Short-domain. Figure (25) shows the dissipation components and the total dissipation for this case. The dissipation shows little change compared to the Short-domain case, which is expected due to the small scale properties.



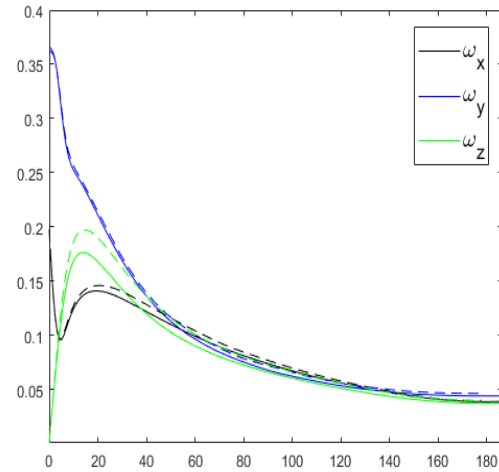
(a) Mean velocity profile.



(b) Rms values of velocity fluctuations.



(c) Viscous, turbulent and total shear stress.



(d) Rms values of vorticity.

Figure 24: Mean velocity profile, rms values of the velocity fluctuations, turbulent-, viscous- and total shear stress, and rms values of the vorticity for the domain size $l_x = 6$ and $l_y = 3$.

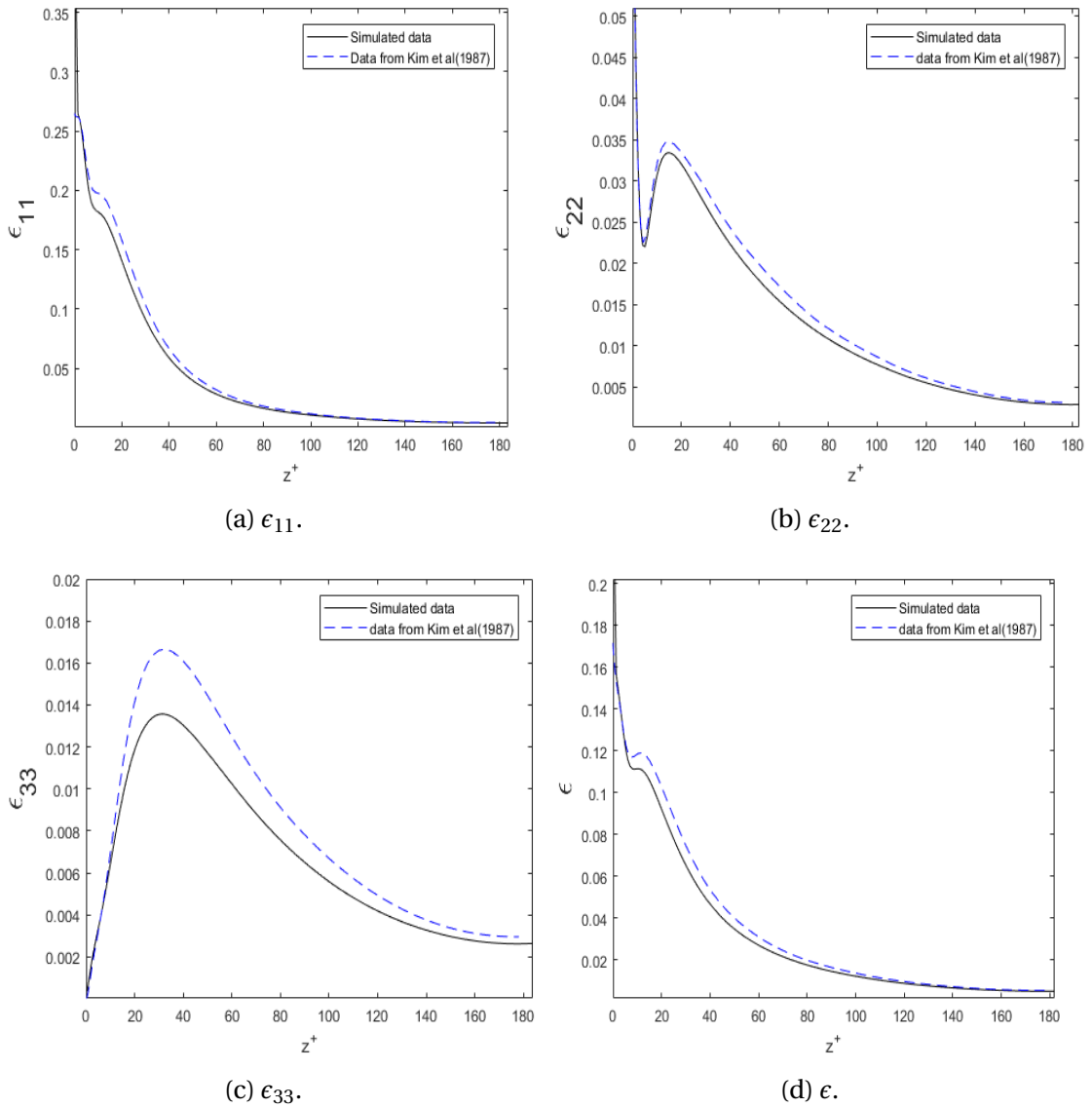
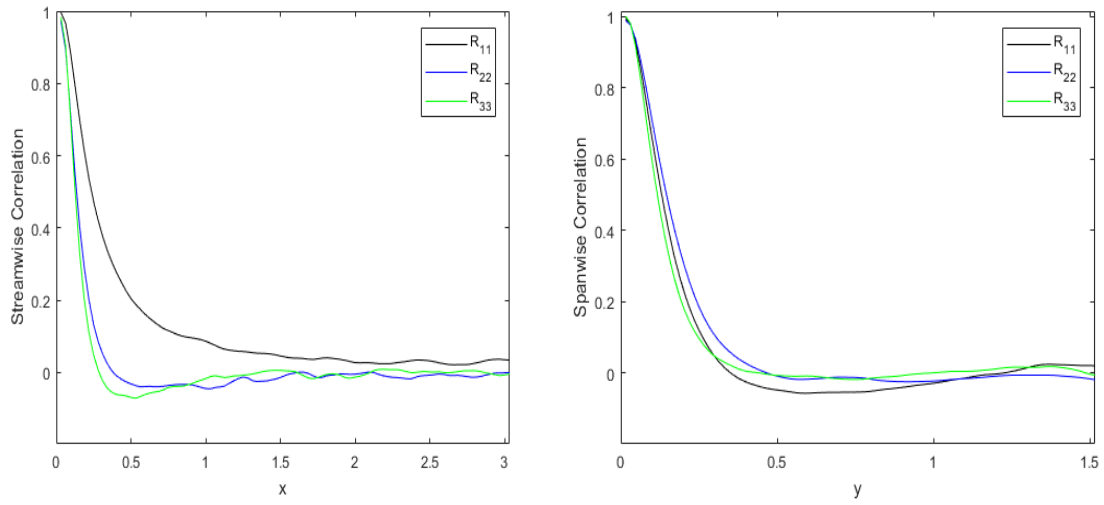


Figure 25: The dissipation components and the total dissipation for the Large-domain case compared with data from Kim et al.

5.4.1 TWO-POINT CORRELATION

Figure (26) shows the two-point correlation of the velocity for the streamwise and the spanwise directions for the domain sizes of $l_x = 6$ and $l_y = 3$, and grid resolution of $192 \times 192 \times 192$. The two-point correlation approaches values close to zero for both directions, which means that the velocities are close to be uncorrelated and that the domain is large enough in both directions.



(a) Two-point correlation in the streamwise direction. (b) Two-point correlation in the spanwise direction.

Figure 26: Two-point correlation for both the streamwise and spanwise directions for domain sizes of $l_x = 6$ and $l_y = 3$.

Part III

DISCUSSION AND CONCLUSION

DISCUSSION

This chapter discusses some of the main results obtained from the Direct Numerical Simulations performed. It will be structured more or less the same way as in the problem formulation, starting with the four cases, discuss the guidelines for required domain size and grid resolution, and briefly suggests further work.

6.1 DISCUSSION

6.1.1 COARSE-GRID SIMULATIONS

In this case the domain size is kept constant equal to $l_x = 1.5$ and $l_y = 0.75$, while the grid resolution increases. The domain size and the grid resolutions used here are considered very small and it is expected to give noticeable discrepancies compared to Kim et al. [1]. The expected behaviour would be that the quantities caused by large scale motion do not change much with increasing grid resolution, while the quantities caused by small scale motion should be affected in an improving manner by finer grid resolutions. For the mean properties and turbulence intensities, which are caused by large scale motion, this reflects for the most part the results obtained, but for the most coarse grid resolution the discrepancy is significant compared to the other simulations. Domain size effect seems to be a secondary effect for the mean velocity profile, for the obvious reason that the domain size is too small.

As stated earlier the vorticity and dissipation are mainly caused by small scale motion and to solve even the smallest scales the grid resolution need to be sufficiently fine. It is clear that the vorticity is affected by increased grid resolution. In the $48 \times 48 \times 192$ simulation the vorticity is significantly better than the other two simulations in z-component. In the other two directions it improves gradually from the most coarse to the finest grid resolution. The dissipation components and the total dissipation all do change significantly with the change of grid resolution. The dissipation component

ϵ_{11} shows small but noticeable changes between the simulations. The component ϵ_{22} shows a strange pattern, with a decreasing value for increasing grid resolution close to the wall and until around $z^+ = 30$ and then they intersect each other. Further away from the wall, $z^+ > 30$, the value increases with increased grid resolution. The last component, ϵ_{33} , increases its value with increasing grid resolution, which is expected. From the theoretic fact that grid resolution should affect small scale motion much more than large scale motion it is possible that for this small domain a secondary effect is occurring and is interfering. This secondary effect seems to be a domain effect, where the domain is too small. Whether it is the length or the width, or both is unknown. This makes the results unpredictable and unreliable.

6.1.2 SHORT-DOMAIN SIMULATIONS

The streamwise component of the grid resolution and the channel length have been doubled two times to see the effects of a longer domain in the streamwise direction. The grid spacing is kept constant, which means that the resolution is the same. Since the grid spacing is kept constant the effect should come from the domain size. The expected outcome is that the turbulence statistics will be unchanged or improving, and therefore get closer to the results obtained by Kim et al.[1]. Some of the quantities will have greater improvement than others due to whether they are large scale or small scale motion. The mean velocity profile has very small changes and has been stable over the course of the simulations, and correspond very well with Kim's results. Another large scale quantity, the rms value of the velocity fluctuations, improved significantly around $z^+ = 10$ to $z^+ = 20$ in the streamwise direction from $l_x = 1.5$ to $l_x = 3$, but when doubled again it did not change noticeably. The other two directions did not show any significant changes. This suggests that the domain sizes in this case ($l_x = 3$ and $l_x = 6$) gives satisfying results.

For the small scale quantities rms value of the vorticity and the dissipation the improvements are noticeable and are gradually getting closer to the results of Kim et al.[1] for increasing values of the channel length. The two simulations with the longest channels are much closer to each other compared to the shortest one ($l_x = 1.5$), which is said to be unreliable and shows signs of grid effect due to the significant discrepancy in dissipation. This is in accordance with what is expected when increasing the domain size and implies that the channel length was too short when $l_x = 1.5$. The two-point correlations for both the streamwise and spanwise directions are clearly getting better after increasing the length of the channel, which means that it is getting more uncorrelated the longer the domain. For the streamwise direction R_{22} and R_{33} are close to zero, but R_{11} is a little bit higher than zero. The two-point correlation in the spanwise direction also gets better with increasing length, but has more discrepancies than in streamwise direction. This shows that the domain still is not

adequate and that the channel width is too narrow and can interfere with the results. The effect of increasing the width will be addressed in the next section.

6.1.3 NARROW-DOMAIN SIMULATIONS

In this case the width of the channel has been doubled two times to see the effect of a wider channel. The other directions have been kept constant and equal to the base grid resolution and domain, which are $48 \times 48 \times 192$ and $l_x = 1.5$, $l_y = 0.75$. To keep the grid spacing constant, the grid resolution in the spanwise direction was also doubled twice. As mentioned in the previous subsection the effect should mainly be the domain size and not grid effect.

The turbulence intensities show small changes in the streamwise direction, and not much in the other two directions. The Reynolds and the viscous shear stress shows insignificant changes. The rms of the vorticity also shows no significant changes with increased channel width, while the dissipation simulations have noticeable differences, although less than for the Short-domain case. Even though the differences between the simulations are not so big, the discrepancies towards the data from Kim et al.[1] are greater than for the Short-domain case. This suggests that the effect of a too short channel is significantly greater than a too narrow channel. The two-point correlation clearly shows that the channel width of the widest channel simulation is adequate. The next section will discuss how the large-domain will affect the results.

6.1.4 LARGE-DOMAIN SIMULATIONS

The domain size in this case is very close to the one used in Kim et al.[1], although with different grid resolution, so the expected results should be close to their results. Even though the DNS code used by both Kim et al.[1] and the one used in this thesis are considered good, they are different and a discrepancy is to be expected.

The mean velocity profile and the turbulence intensities do not show significant discrepancies compared to the short-domain case. This can be interpreted as that the effect of increasing the channel width from the base domain size is insignificant. The Reynolds shear stresses only have small discrepancies around $z^+ = 10$ and $z^+ = 20$ in the Short-domain and Narrow-domain cases compared to the Large-domain case. The rms of vorticity does not show any significant changes compared to the Short-domain case, but in the Narrow-domain case there are discrepancies in both x- and y-components. The dissipation components are not changing much compared with the Short-domain case. Compared to the Narrow-domain there are significant discrepancies for all dissipation components, where the Large-domain case shows sig-

nificantly better results. It cannot be determined in general whether increasing the channel length has a greater effect than increasing the channel width, but by looking at the large scale quantities and the comparisons between the Short-domain and Narrow-domain cases it can be concluded that in these simulations the effect of increasing the channel length is greater than increasing the channel width.

The two-point correlation approaches values close to zero in both the streamwise and spanwise directions for all components, but R_{11} in both directions deviates a little bit while the other two directions are very close to zero. This means that the velocities are close to be uncorrelated and therefore the domain size is considered to be adequate.

6.1.5 GUIDELINES FOR REQUIRED DOMAIN SIZE AND GRID RESOLUTION

From the previous sections it has become clear that increasing the channel length has a greater effect than increasing the channel width. It is also clear that the Large-domain case did not yield significantly better results compared to the two simulations in the Short-domain case. The analysis of the two-point correlations shows that the Large-domain case had an adequate domain size, while the domain sizes for the Short-domain case was less adequate. With this in mind it seems that using both the domain sizes in the Short-domain case, of $l_x = 3$, $l_y = 0.75$ and $l_x = 6$ and $l_y = 0.75$, with corresponding grid resolutions, give satisfying and adequate results. If the cost of the simulations allows, it is still recommended that $192 \times 192 \times 192$ with domain size $l_x = 6$ and $l_y = 3$ is used to be sure that the domain is adequate in both the channel length and width.

6.1.6 FURTHER WORK

A natural continuation of this work would be to increase the Reynolds number and see how it will affect the turbulence statistics. Due to time limitation this task was not done properly and was therefore excluded from the thesis. It is also interesting to see whether the same patterns explained in the previous sections appears when increasing the Reynolds number. Another interesting thing to do would be to use a finer grid resolution and see how much better the results will correspond to Kim et al.[1]. It can also be interesting to use a finer grid resolution while keeping the domain size constant, and then see if the small scale quantities will improve. Further, the Kolmogorov micro scales could be calculated to see how much it deviates from the grid size used in this thesis.

CONCLUSION

The results from the Coarse-grid simulations shows that for the large scale quantities mean velocity profile and rms of velocity fluctuations the two most coarse grid resolutions have a significant discrepancy, while the discrepancy gets smaller with finer resolutions. The Reynolds shear stress shows the same pattern. The small scale quantities, rms of vorticity and dissipation, have significant discrepancies for some of the components. The rms of vorticity improves for increasing grid resolution. The dissipation component ϵ_{11} has insignificant discrepancy. ϵ_{22} has an odd behaviour in that close to the wall it starts to decrease with increasing grid resolution, but going further away from the wall the opposite behaviour occurs. A possible reason is that the domain is so small that the dissipation is affected by the domain size and the data might be unreliable. ϵ_{33} has an expected behaviour with increased value with increasing grid resolution. For the Short-domain and Narrow-domain cases the domain size increases in the streamwise and spanwise directions respectively. The large scale quantities does not change noticeably, but the Narrow-domain case shows a significant discrepancy compared to both Short-domain and Kim et al. The rms of vorticity does not change noticeably in neither Short-domain nor the Narrow-domain case. For the dissipation in Short-domain the two channels have a significant discrepancy towards the shortest channel of length $l_x = 1.5$. This suggests that $l_x = 1.5$ is too short, and that a grid effect occurs. In the Narrow-domain case the dissipation components have less discrepancy compared to each other, but bigger compared to Kim's data, than Short-domain. The two-point correlation shows that the two channels in the Short-domain case deviate a little bit from zero in the streamwise direction and in the Narrow-domain case only the widest channel is adequate in the spanwise direction. The Large-domain case is very close to the domain size used in Kim et al.[1] and shows that both the streamwise and spanwise domain size are adequate. The data obtained in this case are satisfying. The discrepancy between the Large-domain case compared to the two domains $l_x = 3, l_y = 0.75$, and $l_x = 6, l_y = 0.75$ is small. This indicates that both domain sizes in the Short-domain case are satisfying.

Another conclusive remark is that increasing the channel length has a greater impact than increasing the channel width.

BIBLIOGRAPHY

- [1] J. Kim, P. Moin, and R. Moser. Turbulence statistics in fully developed channel flow at low reynolds number. Journal of Fluid Mechanics, 177(1):133–166, 1987.
- [2] Stephen B. Pope. Turbulent Flows. The Press Syndicate of The University of Cambridg UK, 2000.
- [3] Benjamin C. Sebastian. Analysis of data from direct numerical simulation of turbulence. NTNU department of Energy and Process Engineering, 2017.
- [4] Helge I. Andersson. Lecture notes in viscous flows and boundary layers, TEP4156 NTNU, September 2016.
- [5] I. Ertesvåg. Turbulent Strøyming og Forbrenning. Tapir akademisk forlag, Trondheim, 2000.
- [6] Ted D. Bennett. Transport by Advection and Diffusion. John Wiley and Sons, Inc, 2013.
- [7] O. Reynolds. Iv. on the dynamical theory of incompressible viscous fluids and the determination of the criterion. Proceedings of the Royal Society of London. Series A, Mathematical and Physical Sciences, 186(1):123–164, 1987.
- [8] H. Tennekes and L. Lumley. A First Course in Turbulence. The Massachusetts Institute of Technology, 1972.
- [9] S. Corrsin. Interpretation of viscous terms in the turbulent energy equation. J. Aeronaut. Sci. 20, 853, 5(12):853–854, 1953.
- [10] L. Richardson. Weather prediction by numerical process. Cambridge, The University press, 1922.
- [11] Helge I. Andersson. Lecture notes in turbulent flows, TEP4112 NTNU, February 2017.
- [12] J. Kim, R. Moser, and N. Mansour. Database of dns data. <http://turbulence.ices.utexas.edu/data/MKM/chan180/>, December 2001.

- [13] P. A. Durbin and B. Pettersson Reif. Statistical Theory and Modeling for Turbulent Flows. John Wiley Sons, 2011.
- [14] T. Tsukahara, Y. Seki, H. Kawamura, and D. Tochio. Dns of turbulent channel flow at very low reynolds numbers. The 4th International Symposium on Turbulence and Shear Flow Phenomena, At Williamsburg, VA, USA, 2005.
- [15] J. H. Ferziger and M. Peric. Computational Methods for Fluid Dynamics, 3rd Edition. Springer-Verlag, 2002.
- [16] Jurriaan Gillissen. Numerical Simulation of Fibre-Induced Drag Reduction in Turbulent Channel Flow. PhD thesis, Delft University of Technology, 2008.
- [17] Michael Zeltkevic. Adams method. http://web.mit.edu/10.001/Web/Course_Notes/Differential_Equations_Notes/node6.html, April 1998.
- [18] M Brenner. Energy dissipation for isotropic turbulence and taylor's microscale. https://www.seas.harvard.edu/brenner/taylor/handouts/taylor_stats/node3.html#eqfindisl, April 2000.
- [19] G. I. Taylor. Statistical theory of turbulence. Proceedings of the Royal Society of London. Series A, Mathematical and Physical Sciences, 151(873):444–454, 1935.
- [20] N. Mansour, J. Kim, and P. Moin. Reynolds-stress and dissipation-rate budgets in a turbulent channel flow. Journal of Fluid Mechanics, 194(1):15–44, 1988.
- [21] Olav Førde. Analysis of the turbulent energy dissipation. Master's thesis, Norwegian University of Science and Technology (NTNU), 2012.
- [22] Tor Marstein. Direct numerical simulation of turbulent flow in a channel with transverse ribs. Master's thesis, Norwegian University of Science and Technology (NTNU), 2015.
- [23] Lihao Zhao. Particles in wall turbulence. PhD thesis, Norwegian University of Science and Technology (NTNU), 2015.
- [24] P. Saarenrinne and M. Piirto. Turbulent kinetic energy dissipation rate estimation from piv velocity fields. Experiments in Fluids. Springer-Verlag Berlin, 29(1):300–307, 2000.